Politecnico di Torino

Nanotechnologies for ICTs

Master's Thesis Project

ENGINEERED BIOORTHOGONAL NANOCATALYSTS FOR ERADICATED BIOFILMS

Supervisor:
Prof. Valentina Alice Cauda

Supervisor at University of Massachusetts:
Prof. Vincent Martin Rotello

Candidate:
Lucrezia Ferracuti
S241301

October 2019

Considerate la vostra semenza:
fatti non foste a viver come bruti
ma per seguir virtute e canoscenza

Dante Alighieri
La Divina Commedia - Inferno: C. XXVI, v.120

ACKNOWLEDGEMENTS

I would like to thank every person who took part of my experience, mainly supporting me during my last years, the hardest ones from the academic point of view.

Many thanks to Professor Valentina Alice Cauda, my supervisor in Italy, who introduced me with passion in the interesting world of theranostics, being always available and helpful, giving wise advices every time. A big thank to Professor Vincent M. Rotello who gave me the opportunity to interact with one of the world-class researchers and to work in his laboratory "Rotello lab" at the University of Massachusetts. This experience made me grow up from an academic and also personal point of view, meeting new people, sharing opinions, intellectually growing and discovering the american local culture. A special thank goes to the PhD student Rui Huang who guided me from the beginning to the end of my project, fitting me in with the guys of the "Nanozymes" group. Then, thanks to Harini and Bhavna for the support given to me in the lab lightening the hours of work in the lab. I will remember every "sweet" break at UMass bakery and dinners at the Hampshire dining together. And I will never forget our trip to Washington DC where we spent beautiful days together discovering the capital.

My american experience could not have been the same without my friends Mui, Ehsan and Richard. They have been my "american family", I could not imagine the snowy and freezed Amherst without them. Thanks to my friend Ehsan who passed late dinners with me, being always available and kind; a big thank to Richard who shared with me hidden places of Amherst merged to the nature allowing me to know the "real" America. Many thanks to my thai friend Mui for being my friend since we met. I will never forget pleasant weekends spent together and I wish to see her again, maybe in Thailand.

Turning back in Torino I would like to say thanks to my classmates Simone, Maria Chiara and Giuseppe who stayed with me during these years. I could not imagine to bear boring classes and projects at Poli without you guys. Mainly Giuseppe's cakes gave us energies sufficiently to face hours of study otherwise hard to do it. Even though we spent a too little time together, I want to thank my homonymous friend Lucrezia and Giulia who supported me during the first period in Turin, a foreign city for me at that time, when I did not know anybody. Morevore, I would like thank Nicola, Massi and Nicolò for the

pleasant evening spent together, joking and smiling.

Finally, many thanks go to the most important part of my life, my family, who supported me especially during my academic growth from Ancona to Torino. Many thanks to my dad who was my practical support, always ready to put family before all else even though he had his work to think about. Many thanks to my mom who, instead, was the psychological support that everybody should have teaching me that we are strong enough to fight everything. And to conclude, the last but not least thank goes to my sister Federica who was my model since I was 5 years old when I started playing tennis looking at her. Her passion and perseverance to reach the aim inspired me.

Vorrei ringraziare ogni persona che ha fatto parte della mia esperienza, sostenendomi soprattutto durante gli ultimi anni, i più intensi dal punto di vista universitario.

Molte grazie alla Professoressa Valentina Alice Cauda, la mia relatrice in Italia, per avermi introdotto con passione nell'interessante mondo della teranostica, e per essere stata sempre disponibile e d'aiuto, dandomi ogni volta saggi consigli. Un grande grazie va al Professor Vincent M. Rotello il quale mi ha dato la possibilità di lavorare con uno dei ricercatori di livello mondiale accogliendomi nel suo laboratorio "Rotello lab" all'Università del Massachusetts. Questa esperienza mi ha fatto crescere da un punto di vista sia accademico che personale, permettendomi di conoscere nuove persone, scambiare opinioni, crescere intellettualmente e scoprire la cultura locale americana. Un grazie speciale va al dottorando Rui Huang per avermi guidato dall'inizio alla fine del mio progetto, inserendomi tra gli altri ragazzi del gruppo "Nanozymes". Inoltre, grazie a Harini e Bhavna per il supporto che mi hanno dato rendendo le ore di lavoro in laboratorio molto meno faticose. Ricorderò ogni "sweet" break alla pasticceria dell'UMass e le cene al Hampshire dining che abbiamo condiviso. Non dimenticherò mai il nostro viaggio in Washington DC dove abbiamo trascorso insieme fantastici giorni esplorando la capitale.

La mia esperienza americana non sarebbe potuta essere la stessa senza i miei amici Mui, Ehsan e Richard. Sono stati la mia "famiglia americana", non posso immaginare la nevosa e fredda Amherst senza loro. Un grazie va al mio amico Ehsan per aver condiviso con me le tarde cene e per esser stato sempre disponibile e gentile; e un grazie a Richard, che ha condiviso con me i luoghi nascosti di Amherst immersi nella natura, permettendomi di conoscere la "vera" America. Molte grazie alla mia amica thailandese Mui con cui è nata una bellissima amicizia che dura anche a distanza. Non dimenticherò mai i piacevoli weekend passati insieme e spero di rivederci presto, magari in Thailandia.

Tornando a Torino vorrei ringraziare i mie compagni di studi Simone, Maria Chiara e Giuseppe che mi hanno accompagnato in questi anni. Non avrei mai potuto sopportare le noiose giornate al Poli tra lezioni e progetti senza di loro. Soprattutto le torte di Giuseppe ci hanno dato le forze sufficienti per poter affrontare ore di studio altrimenti difficili da sostenere. Anche se abbiamo passato poco tempo insieme, vorrei ringraziare la mia omonima amica Lucrezia e Giulia per avermi supportato durante il primo periodo a Torino, inizialmente sconosciuta, quando ancora non conoscevo nessuno. Inoltre vorrei ringraziare Nicola, Massi e Nicolò per le piacevoli serate che abbiamo trascorso

insieme ridendo e scherzando.

Infine, molte grazie alla parte più importante della mia vita, la mia famiglia, che mi ha supportato e sopportato durante la mia crescita universitaria, da Ancona fino a Torino. Molte grazie a mio padre per essere stato il mio supporto pratico, sempre pronto a mettere la famiglia al primo posto nonostante avesse il suo lavoro a cui pensare. Molte grazie a mia madre per essere stata invece il mio supporto psicologico insegnandomi che si può essere forti abbastanza per poter affrontare tutto. E per concludere, l'ultimo ma non meno importante grazie va a mia sorella Federica che è stata il mio modello fin da quando avevo 5 anni quando ho iniziato a giocare a tennis guardando lei. La sua passione e perseveranza nel raggiungere gli obiettivi mi hanno sempre ispirato.

ABSTRACT

This work describes the Master's Thesis project carried out at the University of Massachusetts, Amherst. The goal of this project is to create selective and effective bioorthogonal nanocatalysts for the treatment of biofilm-associated infections. The antimicrobial activity through the activation of a pro-drug using polymeric nanoparticles encapsulating hydrophobic transmission metal catalysts (TMCs) is analysed.
Bioorthogonal chemistry has emerged as a promising strategy for modulating bioprocesses through reactions that cannot be achieved by natural enzymes and TMC-mediated bioorthogonal catalysis has not been previously demonstrated for the eradication of biofilms.
Based on a previous work [1], the quaternary ammonium polymer ($PONI-C11-TMA$) is used to synthesize polymeric nanoparticles (PNPs) encapsulating iron-porphyrin [Fe(TPP)]Cl and the characterization of dimension and catalytic behaviour, performed by the *in vitro* activation of a resorufin-based pro-fluorophore, are carried out.
Having characterized the activity of the polyzyme (PZ), the bioorthogonal catalysis in GFP-(Green Fluorescent Protein) expressing *E. Coli* biofilms is subsequently probed by confocal microscopy images. The ability of the polyzyme to catalyze chemical reactions in a biological environment is then exploited to activate the non-toxic pro-Moxifloxacin analysing the viability of *E.Coli* (CD-2) biofilms after the treatment.
Based on these preliminary studies, these TMC-loaded polymeric nanoparticles can penetrate biofilms and perform pro-drug activation efficiently to eradicate infections. Polymer-based nano-catalysts or polyzymes feature significant innovations in structure, function and therapeutic applications.
The expectation is that engineering the surface of polyzymes will provide selectivity toward biofilms compared to healthy mammalian cells, reducing side-effects. Furthermore, the ability to perform multi-drug activation will provide enhanced therapeutic efficacy. The polyzyme platform provides a modular toolkit to perform bioorthogonal reactions with precise control while maintaining high efficiency and a potentially powerful tool to combat bacterial biofilm-associated infections.

CONTENTS

I INTRODUCTION 1

1 THERANOSTIC NANOPARTICLES (NPS) 2

1.1 Bioorthogonal Chemistry . . . 3
1.2 Bioorthogonal Transition Metal Catalysts (TMCs) . . . 3
1.3 State of the art . . . 4
1.3.1 Palladium-based Complexes . . . 4
1.3.2 Ruthenium-based Complexes . . . 5
1.3.3 Iron-based Complexes . . . 6
1.4 Advantages and Limitations of bioorthogonal TMCs . 6
1.5 Nanometric scaffolds for TMCs . . . 7
1.5.1 Nanozymes (NZs) . . . 7
1.5.2 Polyzymes (PZs) . . . 8
1.6 Chapter Summary . . . 9

II MATERIALS AND METHODS 10

2 SYNTHESIS 11

2.1 Synthesis of Nanozymes (NZs) . . . 11
2.1.1 Synthesis of 2 nm Au core NPs . . . 11
2.1.2 Monolayer Ligand exchange reaction . . . 13
2.1.3 Encapsulation of TMCs into AuNPs . . . 15
2.2 Fabrication of Polyzymes (PZs) . . . 16
2.2.1 Fabrication of polymeric nanoparticles (PNPs) . 17
2.2.2 Encapsulation of TMCs into PNPs . . . 18

3 CHARACTERIZATION 20

3.1 Characterization Techniques . . . 20
3.1.1 Transmission Electron Microscopy (TEM) . . . 20
3.1.2 Dynamic Light Scattering (DLS) . . . 22
3.2 Kinetic studies . . . 23
3.2.1 Catalytic activity of Nanozymes (NZs) in solution 25
3.2.2 Catalytic activity of Polyzymes (PZs) in solution 27
3.3 Size Characterization . . . 28
3.3.1 DLS and TEM characterization of gold nanoparticles (AuNPs) and nanozymes (NZs) . . . 29
3.3.2 DLS and TEM characterization of polymeric nanoparticles (PNPs) and polyzymes (PZs) . . . 30

III EXPERIMENTAL METHODOLOGY 33

4 BIOFILM PENETRATION USING POLYZYMES (PZS) 34

4.1 Optical Microscopy . . . 34
4.1.1 Confocal Laser Scanning Microscopy (CLSM) . 35
4.1.2 Green Fluorescent Protein (GFP) . . . 37
4.2 Imaging Application of Polyzymes (PZs) . . . 37

4.2.1 Biofilm GFP-expressing *E. Coli* culture 38
4.2.2 Confocal Imaging of biofilms 39
5 BIOORTHOGONAL CATALYSIS IN BIOFILMS 42
5.1 Antimicrobial activity studies 42
5.1.1 MBIC (Minimum Biofilm Inhibitory Concentration) 44
5.1.2 MBEC (Minimum Biofilm Eradication Concentration) 46
5.2 Antimicrobial activity through pro-drug activation using Polyzymes (PZs) 48
5.2.1 Alamar Blue Assay 48
5.2.2 Biofilm *E. Coli* (CD-2) culture 49
5.2.3 Biofilm Viability studies 49
IV RESULTS AND DISCUSSION 52
6 RESULTS AND OUTLOOK 53
6.1 Minimize side-effects by designing a biofilm-targeting polyzyme (PZ) 53
6.1.1 Fabrication and characterization of pH-responsive polyzyme (PZ) 55
6.1.2 Biofilm Study in an *in vitro* co-culture model . . 57
6.2 Maximize therapeutic efficacy by multi-drug activation 58
6.2.1 Selection and Fabrication of pro-drugs 58
6.2.2 Testing of combination therapy 60
6.2.3 Testing of efficacy of combination therapy in an *in vitro* co-culture model 60
7 CONCLUSIONS 61
BIBLIOGRAPHY 62

LIST OF FIGURES

Figure 1 Schematic representation of a theranostic nanoparticle structure [3]. 2
Figure 2 Schematic representation of TMC – mediated bond cleavage reactions. 4
Figure 3 Uncaging reactions of a) propargyl oxycarbonyl protected lysine under physiological conditions in PBS, and b) propargyl oxycarbonyl protected rhodamine in mammalian cells [14]. 5
Figure 4 Development of biofilms [24]. 6
Figure 5 a) Schematic representation of the gold nanoparticle encapsulating TMCs or nanozymes (NZs) b) Pro-drug activation in living cells using nanozymes (NZs). 8
Figure 6 a) Molecular structures of polymer derivatives b) Confocal images of E2-Crimson RFP (Red Fluorescent Protein)-expressing *E. Coli* DH5α biofilm after 1 h treatment with polymer-rhodamine green at 1 μM concentration. Scale bars are 30 μm. 9
Figure 7 Schematic illustration of the inorganic Au core protected by a soft organic monolayer [44]. . . 14
Figure 8 Structure of the monolayer ligand capping the gold nanoparticle (AuNP). 15
Figure 9 Structure of nanozymes based on encapsulating transition metal catalysts (TMCs) in functionalized gold nanoparticles 16
Figure 10 Schematic illustration representing the self-assembling of $PONI-C_{11}-TMA$ polymer into polymeric nanoparticles. 17
Figure 11 Synthesis of the monomer and polymer ($PONI-C_{11}-TMA$). 18
Figure 12 Schematic representation of the encapsulation of the [Fe(TPP)]Cl catalyst in the hydrophobic pocket of the polymer. 19
Figure 13 Schematic representation of Transmission Electron Microscopy (TEM) structure [48]. 21
Figure 14 Setup for Dynamic Light Scattering (DLS) of the Malvern Zetasizer Nano ZS [51]. 23
Figure 15 Schematic representation of the activation of aryl-azide protected resorufin by the catalytic behaviour of the iron-porphyrin metal catalyst. 24

Figure 16 a) Schematic representation of the catalysis mediated by encapsulated Transition Metal Catalyst (TMC), b) Azide reduction reaction catalysed by the catalyst, c) Structure of the iron-porphyrin metal catalyst. 25
Figure 17 Kinetic trends of the iron-porphyrin encapsulated in (a) Au-COOH, and in (b) Au-TTMA nanozymes. 26
Figure 18 Thermo-responsive catalytic behaviour of the Au-TTMA nanozymes. 26
Figure 19 Schematic representation of the activation of the pro-fluorophore mediated by the polyzyme (PZ). 27
Figure 20 Kinetic trends of the iron-porphyrin encapsulated in the polyzyme (PZ). 28
Figure 21 DLS measurements of the a) Au-TTMA and b) Au-COOH nanoparticles. 29
Figure 22 TEM images of the a) Au core, b) Au-TTMA and c) Au-COOH nanoparticles. Scale bars are 50 nm. 30
Figure 23 Characterization of $PONI-C_{11}-TMA$ particles using TEM imaging and DLS measurement 31
Figure 24 Characterization of polyzymes (PZs) using TEM imaging and DLS measurement. 31
Figure 25 Schematic representation of the Confocal Laser Scanning Microscopy (CLSM) structure [47]. . 35
Figure 26 Schematic illustration of the confocal microscopy experiment setup. 39
Figure 27 Confocal microscopy images show successful *in vitro* activation. **I.** GFP (green fluorescent protein)-expressing *E. Coli* (CD-2) biofilms. **II.** Red fluorescence of activated resorufin. **III.** Merged of I and II. **IV.** Pro-resorufin only as control group. Scale bars are 50 µm. 40
Figure 28 Selected antibiotic: Moxifloxacin ($\log(P) = 2.9$). 42
Figure 29 Synthesis of the pro-Moxifloxacin 43
Figure 30 Schematic representation of MBIC/MBEC assay [62]. 45
Figure 31 Biofilm viability test through MBEC (Minimum Biofilm Eradication Concentration) in logarithmic scale. Error bars represent standard deviation. 47
Figure 32 Schematic representation of the activation of pro-Moxifloxacin by using the polyzyme. . . . 48

Figure 33 Biofilms treated with pro-Moxifloxacin (yellow bars), Moxifloxacin (blue bars), pro-Moxifloxacin + polymers (green bars) and pro-Moxifloxacin + polyzymes (red bars). Error bars represent standard deviation. 51
Figure 34 Schematic representation of the pH-responsive polymers (zwitterionic and cationic). 54
Figure 35 Schematic representation of the selective targeting of biofilm infections using pH-responsive polyzymes. 55
Figure 36 Synthesis of the pH-responsive polymer. 55
Figure 37 Schematic representation of biofilm-mammalian cell co-culture model. 57
Figure 38 Selected antibiotics: Sulfamethoxazole (log(P) = 0.89) and Ciprofloxacin (log(P) = 0.28). . . . 59
Figure 39 Synthesis of pro-drugs: pro-Sulfamethoxazole and pro-Ciprofloxacin [74]. 59

LIST OF TABLES

Table 1 List of the chemicals used in the 2 nm AuNP core synthesis. 12
Table 2 Size distribution of Au-TTMA and Au-COOH NPs and NZs recorded by DLS. 29
Table 3 MBIC values evaluated for the polyzyme, Moxifloxacin and pro-Moxifloxacin. 46
Table 4 MBIC and MBEC values evaluated for the polyzyme, Moxifloxacin and pro-Moxifloxacin. 47

ACRONYMS

TMCs Transition Metal Catalysts

Pd Palladium

PBS Phosphate Buffered Saline

Ru Ruthenium

TON Turnover Number

DNA Deoxyribonucleic Acid

FAD Flavin Adenine Dinucleotide

SOG Singlet Oxygen Species

NOX Nicotinamide Adenine Dinucleotide Phosphate Oxidase, NADH oxidase

Fe Iron

[Fe(TPP) Cl]Iron-(Tetraphenyl Porphyrin) Chloride

NZs Nanozymes

EPS Self-Produced Extracellular Polymeric Substances

Au Gold

AuNPs Gold Nanoparticles

PNPs Polymeric Nanoparticles

CB[7]Cucurbit[7]Uril

PZs Polymer Nanozymes

RFP Red Fluorescent Protein

E. Coli Escherichia Coli

TTMA Tetraethylene Glycol Trimethyl Ammonium

COOH Carboxylate

HCl Hydrochloric Acid

HNO_3 Nitric Acid

$HAuCl_4$ Hydrogen Tetrachloroaurate (III) Hydrate

$N(octyl)_4Br(ToAB)$ Tetraoctylammonium Bromide

$C_5H_{12}S$ 1-Pentanethiol

$NaBH_4$ Sodium Borohydride

C_2H_6O Ethanol, EtOH

CH_2Cl_2 Dichloromethane, DCM

CH_3OH Methanol

$(CH_3)_2S$ Dimethyl Sulfide, DMS

C_6H_{14} Hexane

PES Polyethersulfone

MWCO Molecular Weight Cut-Off

$(CH_2)_4O$ Tetrahydrofuran, THF

$C_6H_8O_6$ Ascorbic Acid

$PONI-C_{11}-TMA$ Quaternary Ammonium Polymer

$H_2C_2(CO)_2NH$ Maleimide

C_4H_4O Furan

$(C_2H_5)_2O$ Diethyl Ether

$CH_3CH_2OCH=CH_2$ Ethyl Vinyl Ether

DLS Dynamic Light Scattering

TEM Transmission Electron Microscopy

SEM Scanning Electron Microscopy

SE Secondary Electrons

BSE Backscattered Electrons

PE Primary Electrons

Ag Silver

PCS Photon Correlation Spectroscopy

QELS Quasi-Elastic Light Scattering

D Translation Diffusion Coefficient

NNLS Non-Negative Least Squares

$C_{12}H_7NO_3$ Resorufin

GSH Glutathione

Cu Copper

CLSM Confocal Laser Scanning Microscopy

LCSM Laser Confocal Scanning Microscopy

GFP Green Fluorescent Protein

NA Numerical Aperture

LB Lysogeny Broth

NaCl Sodium Chloride

OD Optical Density

IPTG Isopropyl-β-D-Thiogalactoside

P Partition Coefficient

MBIC Minimum Biofilm Inhibitory Concentration

MBEC Minimum Biofilm Eradication Concentration

TSB Tryptic Soy Broth

$(CH_3)_2SO$ Dimethyl Sulfoxide, DMSO

$C_{12}H_7NO_4$ Resazurin

$C_6H_7NO_3S$ 4-Hydroxybenzenesulfonamide

$C_7H_{16}NO_2Cl$ (3-Carboxypropyl)-Trimethylammonium Chloride

$C_7H_{10}N_2$ 4-Dimethylaminopyridine, DMAP

$C_6H_{15}N$, Et_3N Triethylamine

C_3H_7NO Dimethylformamide, DMF

$C_8H_{17}N_3{\cdot}HCl$ N-Ethyl-N'-(3-Dimethylaminopropyl)Carbodimide Hydrochloride, EDC·HCl

ICP-MS Inductively Coupled Plasma Mass Spectrometry

LDH Lactate Dehydrogenase

DHPS Dihydropteroate Synthase

HPLC High-Performance Liquid Chromatography

FBEC Fractional Biofilm Eradication Concentrantion

Part I

INTRODUCTION

1 THERANOSTIC NANOPARTICLES (NPS)

Theranostic nanosystems have emerged as a useful tool for anticancer and antimicrobial treatments. The term *theranostic* describes the combination of diagnostic and therapeutic efficiency in a single entity and has the potential to significantly enhance the treatment of the desease [2].
The design of nanometric vehicles (e.g. nanoparticles, liposomes, microspheres, *etc*.), which can be loaded with a large amount of drugs and deliver them to specific targets, and the functionalization of these nanosystems by attaching imaging contrast agents, allow to diagnose a desease in individuals and then use identical or closely related agents to treat these deseases [3]. Therefore, theranostic nanoparticles allow for drug delivery, cell targeting and molecular imaging.
The basic structure of these nanosystems (Figure 1) comprises at least three main components:

- **Biomedical payload**: includes imaging and therapeutic agents
- **Carrier**: provides physical protection
- **Surface modifier**: provides additional properties.

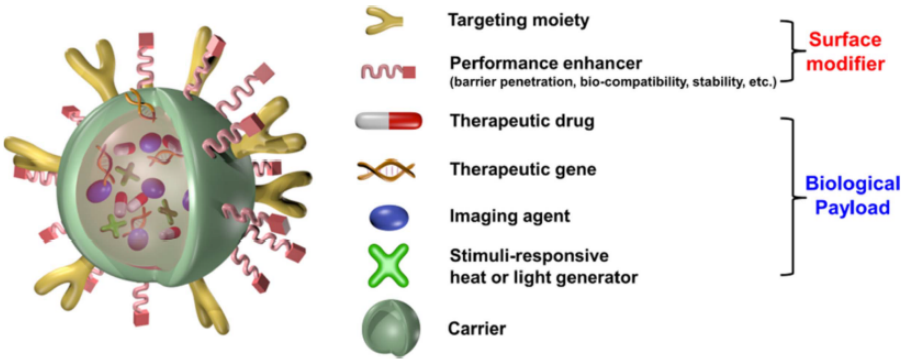

Figure 1: Schematic representation of a theranostic nanoparticle structure [3].

This efficient new targeted therapy exploits nanotechnologies to develop new *non-invasive* therapeutic strategies and it is mainly based on the chemical research. Especially, bioorthogonal chemistry has offered a powerful tool to enhance the functional possibilities of intracellular chemistry catalysing transformations that cannot be naturally performed by enzymes [4].

1.1 BIOORTHOGONAL CHEMISTRY

The concept of bioorthogonal chemistry was first introduced by Bertozzi and coworkers who elucidated on the efficiency of a chemical reaction catalyzed by numerous functional groups present in biosystems including oxidants, reductants, eletrophiles and nucleophiles amidst having a very minimal impact on the surrounding systems [5].

Bioorthogonal chemistry has offered a very valuable connection between chemical biology and organic chemistry that enables biologists in devising tools to understand living systems in new light.
Over the years, numerous strategies have been employed to conjugate the active compound with functional groups that serve as protecting groups. Such a conjugation with the protecting groups will result in the active compound to get converted into its latent state by a process known as *caging*. Originally, studies on protecting groups were focused on simple *click reactions*, which involved redox-sensitive sulfide linkers [6]. One example, that has been extensively discussed, is the use of photolabile functionalities as protecting groups. The photolabile groups can be cleaved under biological conditions to restore their functionality (*uncaging*) at a selective site based on the application. Despite the fact that these light-sensitive reactions are bioorthogonally driven, their activation and efficiency is highly dependent on the nature of the light source [7]. Consequently, if one aims to bring out such uncaging reactions in places that are not easily accessible by light, strategies other than photochemistry needs to be considered.

1.2 BIOORTHOGONAL TRANSITION METAL CATALYSTS (TMCS)

Transition Metal Catalysts (TMCs) offer a very promising role in bringing about bioorthogonal transformations in living systems. Their small size allows the TMCs to localize at regions that are otherwise, almost inaccessible. These advantages have paved way for the application of TMCs in drug delivery, imaging and many other applications [7], [8]. Despite their prominent role, the direct use of TMCs is challenged due to limitations in their nature of biocompatibility and low solubility.

Numerous studies have done to encapsulate TMCs in nanometric scaffolds like nanoparticles or polymeric assemblies. The nanoparticles can further be modified with hydrophobic functionalities, to enhance the biocompatibility and the solubility of these TMCs all the while providing a protective setting for the metal complexes [9].

1.3 STATE OF THE ART

Bioorthogonal chemistry has emerged as a promising strategy for modulating bioprocesses through reactions that cannot be achieved by natural enzymes [10], [11], [5].
Chemical unmasking reactions mediated by transition metal catalysts present a powerful tool for biomedical applications. In this strategy, the conjuation of a biologically active molecule with a caging group can render a loss of function (*masking*); in a designated biological environment, the masked group can then be removed to restore activity via TMC activation (Figure 2). Rather than a one-time, stoichiometric reagent, catalyst molecules are able to remove multiple protecting groups, making this approach much more efficient than installing targeting moieties on bioactive small molecules [12], [7].

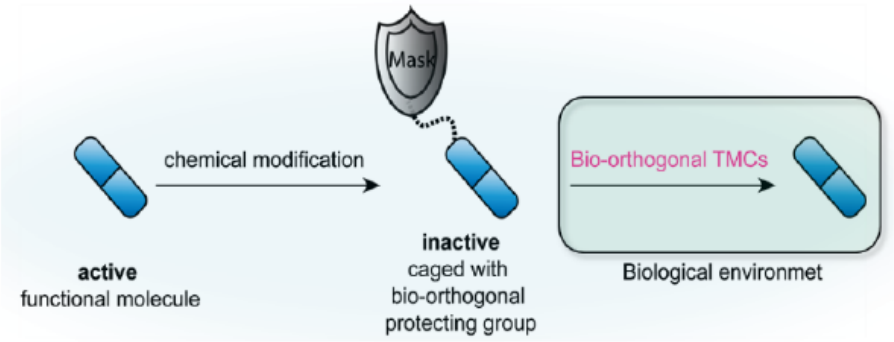

Figure 2: Schematic representation of TMC – mediated bond cleavage reactions.

Several studies have been done over the years to identify transition metal complexes that can bring about efficient uncaging reaction within cells. Some of these findings are discussed below.

1.3.1 *Palladium-based Complexes*

Bradley and coworkers pioneered in reporting the first intracellular reactions catalyzed by functionalized polystyrene microspheres with Pd^0 nanoparticles that were able to enter the living cells and perform bioorthogonal conversions [13].
In a similar study, Chen and coworkers identified organopalladium complexes that are air-stable and the absence of any bulky groups allows them to easily enter the cells [14]. In their study, they demonstrated how palladium metal catalysts can cleave a propargyl group protected lysine derivative to release active lysine (Figure 3).

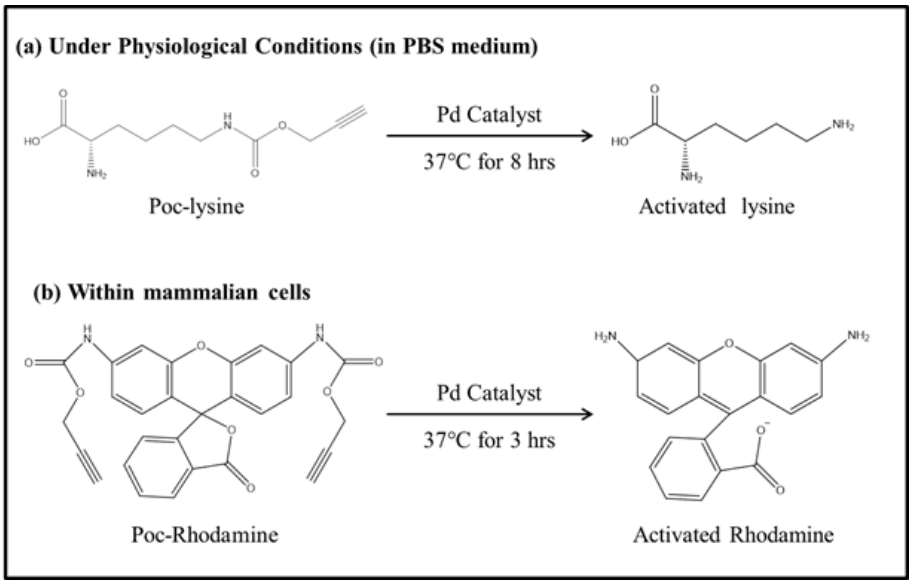

Figure 3: Uncaging reactions of a) propargyl oxycarbonyl protected lysine under physiological conditions in PBS, and b) propargyl oxycarbonyl protected rhodamine in mammalian cells [14].

Independently non-toxic propargyl group protected uracil and Pd^0 microspheres were shown to exhibit anti-proliferative property that was comparable to the active drug used for treatment of pancreatic cancer cells [15].

1.3.2 *Ruthenium-based Complexes*

Some of the earliest works ruthenium (Ru) as catalyst came from Streu and Meggers who reported the ability of the Ru-complexes to cleave allylcarbamate protected amines inside the cells [8]. However, the lower efficiency and turnover number (TON) of catalysis alongside the use of a toxic additive, like thiophenol, made this approach less suited for further application.
Sanchez and coworkers studied on the ability of Ru-complexes to carry out bioorthogonal uncaging to control DNA binding [16].
Recently, Castro and coworkers reported on the photocatalytic activition of Ru-based complexes in the presence of flavin adenine dinucleotide (FAD) and flavoproteins by the generation of singlet oxygen species (SOG) and nicotinamide adenine dinucleotide phosphate oxidase (NADH oxidase, NOX) [17].
Althought these catalysts show potent activity, one of the greatest challenges in maintaining their catalytic nature is the presence of minimal quantities of thiols that can deactivate the catalysts under highly protic environments.

1.3.3 *Iron-based Complexes*

Samsal and coworkers reported the use of a robust catalyst containing Fe-porphyrin to reduce organic azides to amines [18]. Upon screening of a number of Fe-porphyrin derived complexes, they concluded that iron-(tetraphenyl porphyrin) chloride [Fe(TPP)]Cl, was able to easily catalyze the reduction to amines with the same efficiency even in the presence of thiols and highly protic solvents and in biological conditions.
Meanwhile, Prof. Rotello and coworkers employed these Fe-based metal complexes to encapsulate them into nanometric scaffolds and contrive nanozymes (NZs) to perform catalysis similar to naturally occurring enzymes [19], [20], [21]. The Fe-porphyrin catalysts were preferred over the Ru-based catalysts due to comparatively lower toxicity of the Fe-porphyrin catalysts.

1.4 ADVANTAGES AND LIMITATIONS OF BIOORTHOGONAL TMCS

Bacterial infections are a serious threat to public health and the majority of human bacterial infections (~ 80 %) are associated with biofilm formation on living tissue [22]. Biofilms are aggregates of microorganisms, in which bacterial cells are embedded in self-produced extracellular polymeric substances (EPS) [23].

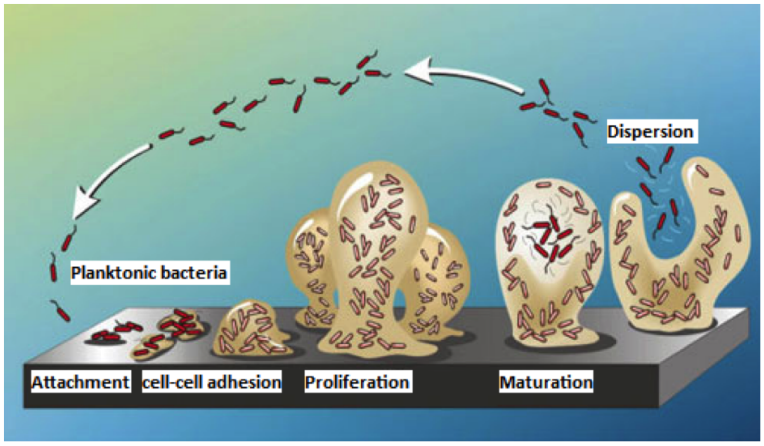

Figure 4: Development of biofilms [24].

Bacterial biofilm formation (Figure 4) results in persistent infections on wounds, implants and indwelling medical devices, including urinary catheters, arthro-prostheses and dental implants [25]. These biofilm infections are highly refractory to antibiotics compared to their planktonic counterparts, as the EPS provides structural stability and protection to bacterial cells.

Susceptibility tests have shown that bacterial biofilms can survive treatment with antibiotics at concentrations 10 to 100-fold the minimum inhibitory concentration of free-floating bacteria. While high doses of antibiotic would ensure the complete elimination of the infection, this would result in severe side-effects in mammalian cells [26].
TMC-mediated uncaging reactions have the potential to remedy this problem due to their ability to generate functional molecules *in situ*. Using this strategy, non-toxic antibiotic precursors can be activated locally at infection site as long as TMCs are designed to target biofilms. Catalyst molecules provide multiple turnovers and are therefore attractive with respect to long-term therapy.

The direct application of TMC-mediated catalysis in biofilm treatment is challenging due to their solubility, limited lifetime and poor penetration ability [13], [27], [8]. The EPS matrix contains polysaccharides, proteins and DNA originating from the microbes, leading to significantly decreased catalytic efficiency in TMCs. In addition, the dense and amphiphilic nature of EPS matrix hinders the penetration of catalyst molecules [28], [29].

1.5 NANOMETRIC SCAFFOLDS FOR TMCS

The most challenging task of improving the metal catalyst solubility, led to the consideration of bringing about covalent or non-covalent modifications of TMCs. Since the TMCs are hydrophobic in nature, numerous approaches were investigated to link these TMCs covalently to hydrophilic ligands or by linking them to charge-modified ligands [30], [31], [32].
Wei and coworkers defined TMC encapsulated nanomaterials as "nanozymes" with enzyme-like caliber [33], [34].
Nanozymes formulated by encapsulating the metal catalysts into nanometric scaffolds was reported by Prof. Rotello and coworkers that provided stability to the catalyst and can also alter the catalyst activity up to some extent. Two kind of nanozyme was designed by them: 2 nm gold core nanoparticles (AuNPs) and polymeric nanoparticles (PNPs) encapsulating TMCs.

1.5.1 *Nanozymes (NZs)*

Prof. Rotello and coworkers dealt with the use of gold nanoparticles (AuNPs) with a core size of 2 nm, the surface of which is further functionalized with a range of ligands with varying chain lenghts and charges. The functionalized AuNPs had an overall length of ~ 10 nm approximately [35]. This approach promotes better results due to the

ability of the nanozymes (NZs) to bring about confined catalysis. Prof. Rotello and coworkers demonstrated the ability of a gold nanoparticle encapsulating ruthenium and palladium functionalized using host-guest chemistry by cucurbit[7]uril (CB[7]) to activate pro-drugs at the site of action [4] (Figure 5).

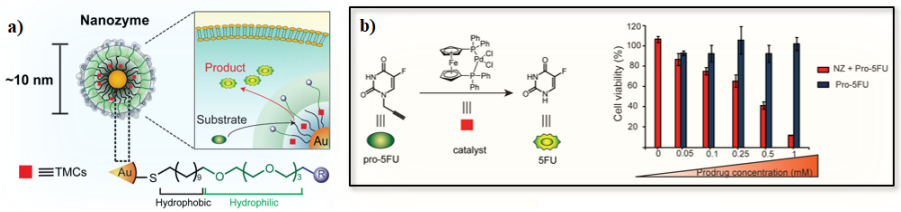

Figure 5: a) Schematic representation of the gold nanoparticle encapsulating TMCs or nanozymes (NZs) b) Pro-drug activation in living cells using nanozymes (NZs).

Nanoparticles have an enormous scope for tuning their surface nature that can prove to be an excellent platform to encapsulate a variety of transition metal catalysts [36]. There are also known to assist both heterogeneous and homogeneous catalysis in the same manner. Moreover, studies have also shown that the products of reactions catalyzed by such nanozymes can easily be separated by simple filtration techniques [37].

1.5.2 *Polyzymes (PZs)*

Prof. Rotello and coworkers reported a modular strategy for the solubilization and protection of hydrophobic TMCs using nanometric scaffolds such as polymeric nanoparticles (PNPs). These nanomaterials are featured with an alkane chain to provide a hydrophobic inner shell to encapsulate TMCs and thereby preserving original TMC activity. Furthermore, this encapsulation strategy can provide a protective environment and impart sustained usability [35].
The terminal interacting unit of these nanometric scaffolds can also be engineered to localize with targeted tissues and cellular environments [38]. Prof. Rotello and coworkers demonstrated the ability of cationic polymeric nanoparticles to penetrate biofilm using rhodamine green functionalized polymer $C_{11} - TMA$ [1](Figure 6).

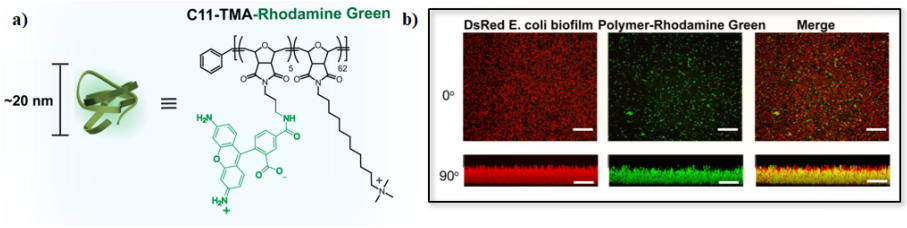

Figure 6: a) Molecular structures of polymer derivatives b) Confocal images of E2-Crimson RFP (Red Fluorescent Protein)-expressing *E. Coli* DH5α biofilm after 1 h treatment with polymer-rhodamine green at 1 μM concentration. Scale bars are 30 μm.

Oxanorbornene-based polymers are appealing because they grow through living polymerizations and are thus capable of providing well-controlled polymers of similar length [39], [40]. In addition, the synthetic scalability provides a key advantage over other nanometric scaffolds.

1.6 CHAPTER SUMMARY

- **Chapter 2**: the chapter is dedicated to the description of the synthesis of gold core nanoparticles/nanozymes and polymeric nanoparticles/polyzymes;
- **Chapter 3**: characterization results of the syntesized nanoparticles and nanozymes are here exposed analyzing dimensions and the catalytic behaviours of the nanocatalysts;
- **Chapter 4**: the ability of the polyzyme to create a path inside the EPS matrix of the biofilm to allow the penetration of TMCs inside it is here shown by confocal images;
- **Chapter 5**: bioorthogonal catalysis in biofilms performed by the polyzyme resulting in the eradication of the biofilm is here reported;
- **Chapter 6**: the chapter is focused on the future improvements that can be carried out based on the obtained results. The functionalization of these nanocatalysts and the multidrug activation can broaden the therapeutic efficacy of the polyzymes;
- **Chapter 7**: general conclusions are discussed in this chapter showing the great application prospective that such a nanocatalyst can have to combat bacterial biofilm-associated infections.

Part II

MATERIALS AND METHODS

2 SYNTHESIS

This chapter is dedicated to the synthesis of nanoparticles analyzed in this project. Especially, procedures related to the synthesis of gold nanoparticles (AuNPs) and polymeric nanoparticle (PNPs) are initially shown. Afterwards, the encapsulation of transition metal catalysts (TMCs) inside the nanometric scaffolds is carried out.

2.1 SYNTHESIS OF NANOZYMES (NZS)

Gold nanoparticles (AuNPs) have recently emerged as a useful tool for effective therapy. Both chemical and physical properties allow to exploit AuNPs as carriers for delivery of drug and gene into specific targets. The inert gold core defines the stability and non-toxicity of the system, while the monolayer allows tuning of surface properties such as charge and hydrophobicity.
The functionalization of AuNPs with thiols linkages provide an effective and selective means of controlled intracellular release [41].

In this section the AuNPs with core diameter of $\sim 2\,nm$ were synthesized and a post-functionalization with a monolayer of tetraethylene glycol trimethyl ammonium (TTMA) and carboxylate (COOH) ligands was performed generating structures with an overall size of $\sim 10\,nm$.
Gold nanoparticles ($2\,nm$) were synthetised by using the *Brust-Schiffrin two-phases method* and further functionalized by the *ligand place-exchange reaction method* developed by Murray [42].
Afterwards, the nanometric scaffold were used to encapsulate the transition metal catalyst (TMC) obtaining the final nanocatalysts named nanozymes.

2.1.1 *Synthesis of* $2\,nm$ *Au core NPs*

In this project the Au core synthesis was performed by following the Brust-Schiffrin protocol for two-phase methodology. This strategy allows the growing of metallic clusters with the simultaneous attachment of self-assembled thiol monolayers on the growing nuclei [43].
All glass wares and stir bars were washed with aqua regia in order to be sterilized before to be used. Aqua regia was prepared by mean of the reaction between hydrochloric acid (HCl) and nitric acid (HNO_3) with a ratio of $3:1$ respectively.

During this procedure no metal spatulus was used to avoid any metal reaction.
The Table 1 shows all chemicals required for the Au-core synthesis specifying the right dose for each of them.

Table 1: List of the chemicals used in the 2 nm AuNP core synthesis.

CHEMICAL NAME	DOSE
Hydrogen Tetrachloroaurate	1 g, 2.9 mmol
Tetraoctylammonium Bromide	3.218 g, 5.9 mmol
1-Pentanethiol	0.613 g, 5.9 mmol
Sodium Borohydride	1.113 g, 29.43 mmol

The hydrogen tetrachloroaurate (III) hydrate ($HAuCl_4$) solution was obtained by dissolving $HAuCl_4$ (1 g, 2.9 mmol) in 150 mL of MilliQ water in a round bottom flask obtaining a yellow aqueous solution.
A solution of tetraoctylammonium bromide ($N(octyl)_4Br$(ToAB)) was prepared by mixing the phase-transfer reagent (3.218 g, 5.9 mmol) and 340 mL of toluene. The organic phase mixture was then added to the gold solution and a change of the colour from yellow to orange was noticed within a few seconds.
After being stirring for 15 min at room temperature, the two-phase mixture showed a changing in the colour that turned into a dark orange. The stirring phase is crucial in this procedure, the stirring velocity determines the size of the nanoparticles: a fast stirring gives a smaller average Au core size. During this phase, all $HAuCl_4$ was transferred into the organic layer.
Maintaining the two-phase mixture still stirring, 1-Pentanethiol ($C_5H_{12}S$) (0.73 mL) was added dropwise to the mixture with a speed of 1 drop/min. When all the pentanethiol was dropped in the solution, a white colour of the mixture was noticed.
Sodium borohydride ($NaBH_4$) (1.113 g, 29.43 mmol) was dissolved in minimal water and then sonicated to dissolve all the sample. The freshly prepared solution was then added to the mixture quickly changing immediately the colour to black. The two-phase mixture was left stirring vigorously overnight.
The final solution was then transferred to a pH-balanced separating funnel to separate the organic phase containing the Au core from the aqueous phase. After that, the toluene was evaporated in vacuo by means of a rotary evaporator reducing the volume of the solution to 10 mL approximately and increasing its density.
The organic phase mixture was transferred into 50 mL centrifuge tube and the washing procedure was carried out. This step requires the filling of the tube with ethanol (C_2H_6O, EtOH) to precipitate out the

AuNPs and a subsequent centrifugation with 4000 rpm for 10 min at 10 °C. The washing procedure was repeated 20 times to remove excess thiols.
After that, the supernatant solution was discarded and the solid samples were collected into a glass vial by dissolving it in minimal quantities of dichloromethane (CH_2Cl_2, DCM) followed by drying them with nitrogen.

2.1.2 *Monolayer Ligand exchange reaction*

The obtained 2 nm Au core NPs were then post-functionalized using the ligand place-exchange reaction method developed by Murray [42]. In particular, a monolayer of tetraethylene glycol trimethyl ammonium (TTMA) and carboxylate (COOH) ligands were chosen for the surface functionalization of the AuNPs. Prof. Rotello and coworkers synthesized TTMA and COOH ligands used to functionalize gold nanoparticles used in this study. According to this strategy nanoparticles and ligands was taken into account with 1 : 3 ratio respectively.

First, the gold core NPs (30 mg) and ligands (90 mg) were measured. DCM and methanol (CH_3OH) were purged with nitrogen: this procedure was used in order to remove oxygen that can cause oxidation of Au cores eventually causing aggregation.
The ligand sample was dissolved in 2 mL each of the purged DCM and methanol and then sonicated for 5 s in order to guarantee complete dissolution of the sample. While Au core was dissolved in 4 mL of dryed dimethyl sulfide ($(CH_3)_2S$, DMS). The gold solution was left stirring.
The ligand solution was then slowly added to the stirring Au core sample by using a glass pipette. The solution mixture was then purged with nitrogen for 1 min, sealed with parafilm to guarantee the absence of oxygen and finally wrapped with aluminium foil due to the photosensitivity of the sample.
The ligand exchange reaction was then carried out for 3 days under continuous stirring and constantly checked throughout the period for any precipitates.
After that, the solvent was removed from the vial and the AuNPs were washed with purged hexane (C_6H_{14}). This first washing procedure was repeated 6 times by using the centrifuge with a speed of 5000 rpm for 5 min. Then Au core NPs were subjected to a second washing phase with different ratios of hexane:DCM (9:1, 8:1, 7:1, 6:1, 5:1, 4:1, 3:1, 2:1 and 1:1). The solubility of the sample was checked and a final washing with pure DCM was done.
In order to dry the sample, AuNPs were purged with nitrogen and then the solvent was completely evaporated in vacuo by using the rotary evaporator for 2 h.

When the solvent was completely removed, the nanoparticles were immediately dissolved in 10 mL of MilliQ and then vortexed. Further, the aqueous solution of nanoparticles was purified by dialysis with distilled water. To do that, first the nanoparticle solution was taken into a syringe and then passed through a PES syringe filter (0.22 µm pore size) to remove bigger impurities.
Finally, the sample was transferred into a dialysis membrane (10 000 MWCO) and subjected to dialysis in MilliQ water for 4 days changing the water periodically removing the excess of ligands.

The previous explained procedure were perfomed for both ligands leading to the fabrication of Au-TTMA and Au-COOH nanoparticles. The final structure of the monolayer-protected gold nanoparticles is here shown by a schematic illustration (Figure 7).

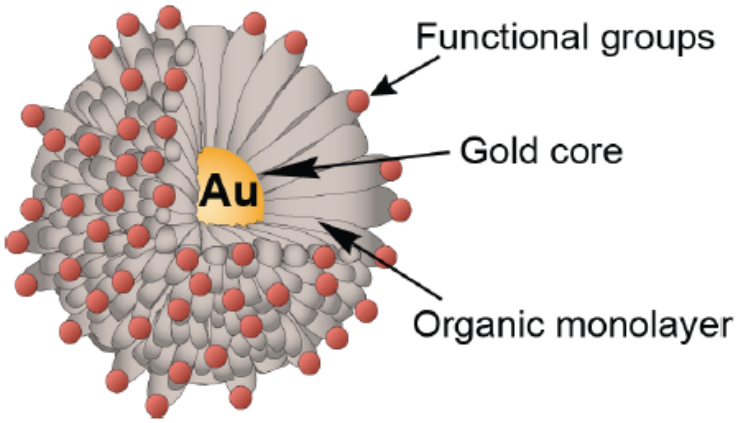

Figure 7: Schematic illustration of the inorganic Au core protected by a soft organic monolayer [44].

In particular, in this project, AuNPs were modified by functionalizing the surface with two different ligands: a monolayer of tetraethylene glycol trimethyl ammonium (TTMA) and carboxylate (COOH) ligands respectively. Each ligand has three distinct regions [9] in its structure (Figure 8):

- an inner hydrophobic aliphatic chain, which provides a favorable environment for catalyst encapsulation
- a hydrophilic tetra(ethylene glycol) chain, which provides biocompatibility to the system
- a terminal charge-containing functional group that determines the nature of interaction of the nanoparticles.

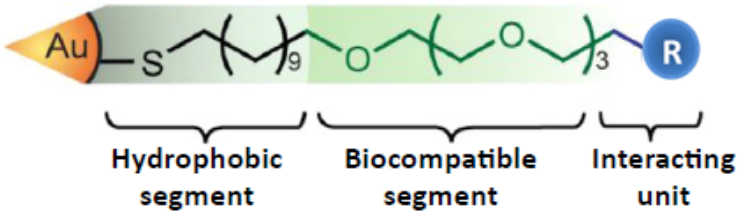

Figure 8: Structure of the monolayer ligand capping the gold nanoparticle (AuNP).

2.1.3 *Encapsulation of TMCs into AuNPs*

In this section gold nanoparticles (AuNPs) scaffolds were used to incorporate transition metal catalysts (TMCs) developping nanozymes able to perform bioorthogonal reactions [4].
In this project, 5, 10, 15, 20-tetraphenyl-21H,23H-porphine(TPP) iron(*III*) chloride [Fe(TPP)]Cl was chosen as the metal catalyst embedded in the nanometric scaffold due to its high turnover number (TON).

First, 10 μM of AuNP solution was prepared by diluting the stock solution in 3 mL of MilliQ water. The metal catalyst was prepared by dissolving 6 mg of the iron-porphyrin (Fe[TPP]Cl) in 3 mL of tetrahydrofuran ($(CH_2)_4O$, THF) and then sonicated to dissolve the catalyst completely.
Afterwards, the hydrophobic catalyst was aspirated into a syringe and added dropwise into the AuNP solution while constantly mixing. The solution became turbid due to the precipitation of the metal catalyst.
After mixing AuNP with the catalyst, the solution was then subjected to vortex allowing the catalyst to interact with the hydrophobic part of the ligand and get encapsulated in monolayers. The remainder of the hydrophobic catalysts precipitated. The toxic THF was completely removed from the sample using the rotary evaporator.
The precipitate was removed by filtration: the sample was collected into a syringe and passed it through a PES syringe filter (0.22 μm pore size). Then, multiple filtrations through a centrifuge filter units with a molecular cutoff of 10 000 were executed to remove free catalysts. The purification was done by using a centrifuge with a speed of 6000 rpm for 5 min. This procedure allows the water to go out through the filter reducing to half the overall volume of the sample.
At the end of any centrifugation procedure, MilliQ water was added to the unit to bring the volume back to the maximum possible limit and centrifuged again. The washing steps were repeated 6 times.
After this purification procedure, another washing phase was performed by preparing 6 mg/mL concentration of ascorbic acid ($C_6H_8O_6$) in MilliQ water and it was used to wash the sample for two times.

Finally, the sample was collected, purged with nitrogen and wrapped with parafilm in order to guarantee absence of oxygen in the sample. Figure 9 shows the schematic structure of a nanozyme obtained by the encapsulation of a transition metal catalyst (TMC) in a nanometric scaffold.

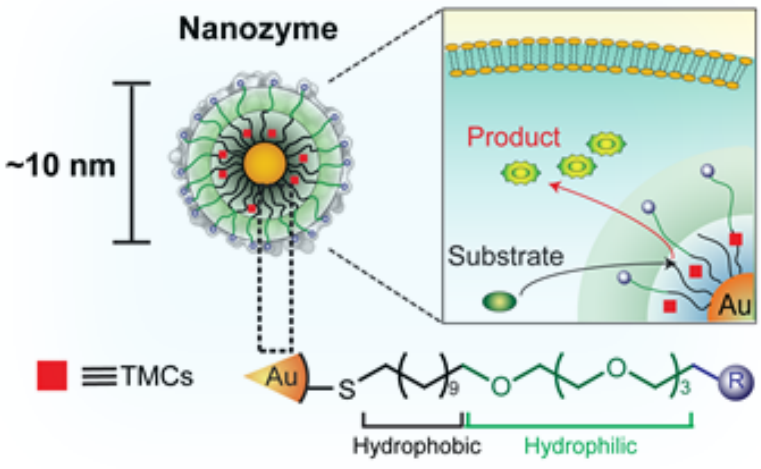

Figure 9: Structure of nanozymes based on encapsulating transition metal catalysts (TMCs) in functionalized gold nanoparticles

2.2 FABRICATION OF POLYZYMES (PZS)

In recent years, polymer-based scaffold has also been found to be an excellent system to encapsulate metal catalysts. The easily tailorable backbone and the dynamic nature of the polymer chains have been studied to alter the extent of catalyst encapsulation and their resulting catalytic efficiency [45].
Although the use of polymers in bioorthogonal chemistry has not introduced a greater influence, taking into account the scope for modification possible in its structure, these systems hold preeminent advantages. The biocompatibility and the non-toxicity of the polymers can be exploited to fabricate polyzymes (PZs) and to be a good alternative to gold core nanozymes (AuNZs).

Prof. Rotello and coworkers designed and synthesized polymeric nanoparticles (PNPs) tuning their therapeutic activity by engineering the hydrophobic and cationic domains incorporated in the synthetic semirigid polymeric scaffold. In particular, a library of quaternary ammo-

nium poly(oxanorborneneimides) were synthesized by varying hydrophobic moieties and their antimicrobial activity was analysed. According to these results, the quaternary ammonium polymer ($PONI-C_{11}-TMA$) showed high efficacy in the biofilm penetration and eradication without affecting mammalian cells [1]. For this reason the hydrophobic C_{11} alkyl chain which bridges cationic headgroup and polymer backbone was exploited to synthesized PNPs studied in this project.

2.2.1 *Fabrication of polymeric nanoparticles (PNPs)*

Prof. Rotello and coworkers synthesized the quaternary ammonium polymer ($PONI-C_{11}-TMA$) that was used for the fabrication of the polyzyme analysed in this project. It was found that polymers containing a bridged C_{11} alkyl chain spontaneously self-assemble into cationic polymeric nanoparticles (PNPs) in aqueous solution (Figure 10) [1].

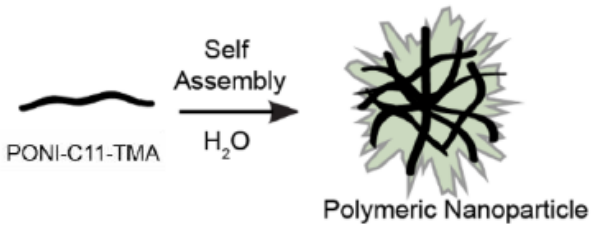

Figure 10: Schematic illustration representing the self-assembling of $PONI-C_{11}-TMA$ polymer into polymeric nanoparticles.

The synthesis of the polymer-based scaffold is here explained. The synthesis of the polymer $PONI-C_{11}-TMA$ starts from the monomer synthesis (Figure 11) [1].

The oxanorbornene derivative **1** was synthesized by *Diels-Alder cycloaddition* adding maleimide ($H_2C_2(CO)_2NH$) and furan (C_4H_4O) to diethyl ether ($(C_2H_5)_2O$). The sample was sealed and heated at 100 °C overnight.
After that it was cooled to room temperture and in order to isolate **1**, the solid was removed, filtered and finally washed with diethyl ether. By a substitution reaction between **1** and alkyl bromide the structure **2** was obtained. The final structure of the monomer **3** was realized via the *Appel reaction* on **2**.
Starting from the final monomer structure, the polymer synthesis was carried out. The monomer **3** was dissolved in purged DCM and Grubbs *3rd* generation catalyst was dissolved in DCM by using a

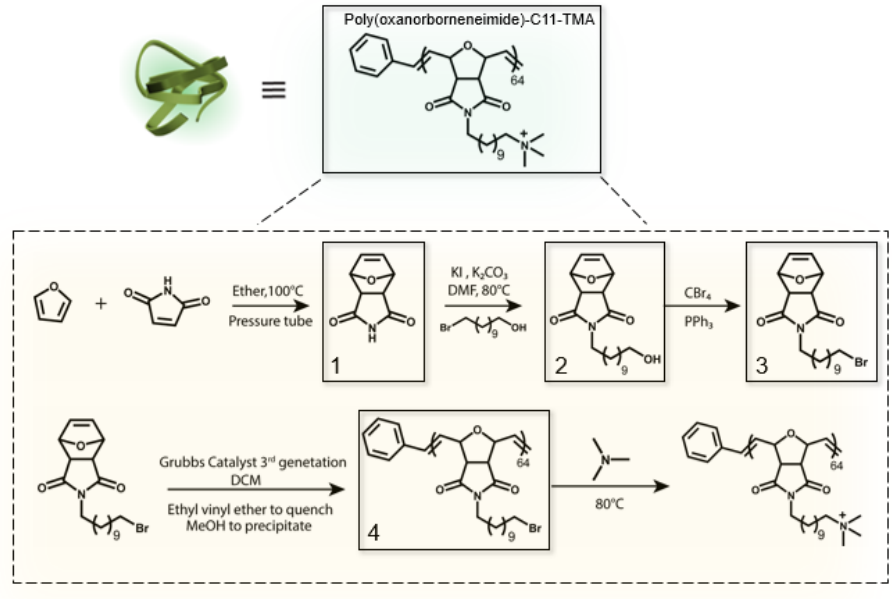

Figure 11: Synthesis of the monomer and polymer ($PONI-C_{11}-TMA$).

separate flask [46]. Both flasks were first sealed and attached to nitrogen and then underwent freeze-pump thaw 3 times and warmed reaching the room temperture. Grubbs *3rd* generation catalyst was syringed out and transferred quickly to the flask containing **3**. After 10 min for the reaction, ethyl vinyl ether ($CH_3CH_2OCH=CH_2$) was added and allowed to stir for 15 min.
The product was obtained by precipitating the sample into a heavily stirred solution of hexane. To purify the product, filtration and dissolution of precipitated polymer into THF were performed. To generate the quaternary ammonium polymer, the polymer **4** was coupled with tertiary amine and purged with nitrogen. The solution was left stirring for 30 min at 80 °C and overnight at 50 °C.
After removing all the solvent, the sample was washed with hexane 2 times and, by using a minimal amount of water, the sample was transferred into a dialysis membrane (10 000 MWCO) and subjected to dialysis in MilliQ water for 3 days changing the water periodically. The polymer was then filtered through PES syringe filters (0.22 µm pore size) and freeze-dried to get all the quaternary ammonium polymers **5**.

2.2.2 *Encapsulation of TMCs into PNPs*

The fabrication of the polyzyme (Figure 12) was carried out by encapsulating the [Fe(TPP)]Cl catalyst into the polymeric scaffold ($PONI-C_{11}-TMA$). The same procedure previously used for the fabrication

of nanozymes (Section 2.1.3) is here exploited.

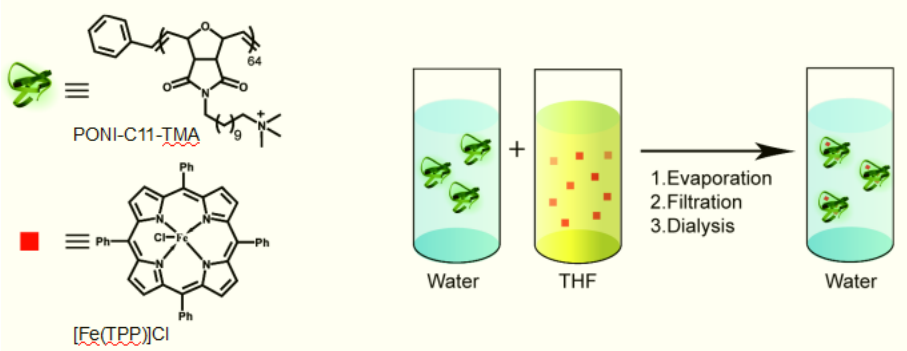

Figure 12: Schematic representation of the encapsulation of the [Fe(TPP)]Cl catalyst in the hydrophobic pocket of the polymer.

Enough polymer ($PONI-C_{11}-TMA$) was dissolved in 2 mL of water to make 1 mM of solution and then stirred vigorously. 5, 10, 15, 20-tetraphenyl-21H,23H-porphine(TPP) iron(III) chloride [Fe(TPP)]Cl (1 mg) was dissolved in 1 mL of THF and it was sonicated to dissolve the catalyst completely. Then, the iron-porphyrin catalyst was aspirated into a syringe and added dropwise into the polymer solution while constantly mixing.
Since the mixture of the two solutions is photosensitive, the sample was wrapped with aluminum foil and then stirred overnight to favor the encapsulation of the catalyst in the hydrophobic pocket of polymers.
The sample was then purged with nitrogen until all the solvent was removed and then dissolved in 2 mL of water and vortexed to resuspend crude polyzymes.
The sample was then taken into a syringe and passed it through a PES syringe filter (0.22 µm pose size). This filtration procedure was perfomed 5 times in order to guarantee that all precipitated catalyst was removed.
Successively, the sample was transferred into a dialysis membrane (10 000 MWCO) and subjected to dialysis in MilliQ water for 4 days to remove any unbound catalyst changing the water periodically.

3 CHARACTERIZATION

In this chapter a brief description of the tools used to characterize gold nanoparticles (AuNPs), nanozymes (NZs), polymeric nanoparticles (PNPs) and polyzymes (PZs) is exposed.
The second part of the chapter shows experimental results about the catalytic behaviour of the nanozymes followed by size distribution analysis of them.

3.1 CHARACTERIZATION TECHNIQUES

This section is focused on the description of the techniques used in order to get information about the size and dimension of nanoparticles synthezised in the Section 2.
Dynamic Light Scattering (DLS) has been exlpoited in order to get the average size of nanostructures and to detect an undesirable aggregation. While, in order to get a more precise value of the dimension, Transmission Electron Microscopy (TEM) has been used.

3.1.1 *Transmission Electron Microscopy (TEM)*

Transmission Electron Microscopy (TEM) is one of the most used characterization techniques that takes advantage from the electrons transmitted through the sample.
Differently from the Scanning Electron Microscopy (SEM), which exploits secondary electrons (SE) and backscattered electrons (BSE), TEM uses primary electrons (PE) to analyze the sample.

The beam of electrons, emitted by the source, is forced to impinge on the specimen that is most often an ultra-thin section less than $100\,nm$ thick. Indeed, TEM requires samples that have to be very thin but also stable enough to withstand the transmission of electrons. The collision generates, on the other side of the sample, transmitted electrons and scattered electrons coming from the elastic scattering due to diffraction.
In order to analyse the top surface and get a high resolution image (up to $0.2\,nm$) of the sample, the structure to be characterized has to be thinned up to $100-200\,nm$ starting from a mm structure. For this reason TEM is considered an *invasive technique* and a sample prepara-

tion has to be required.
There are many techniques that can be used in order to reduce the thickness of the sample; the method is chosen according to the type of materials and the information that is wanted to get from it. For example, it is possible to use first a *mechanical thinning* that exploits nanostructures distributed on a wheel that is able to be spinned getting thinning/ablation of the sample. Then, the sample can further be thinned by *ionic thinning* by using a system of ion milling that exploits an ion source of Ag ions that are accelerated by two electrodes towards the sample reaching high kinetic energies [47].

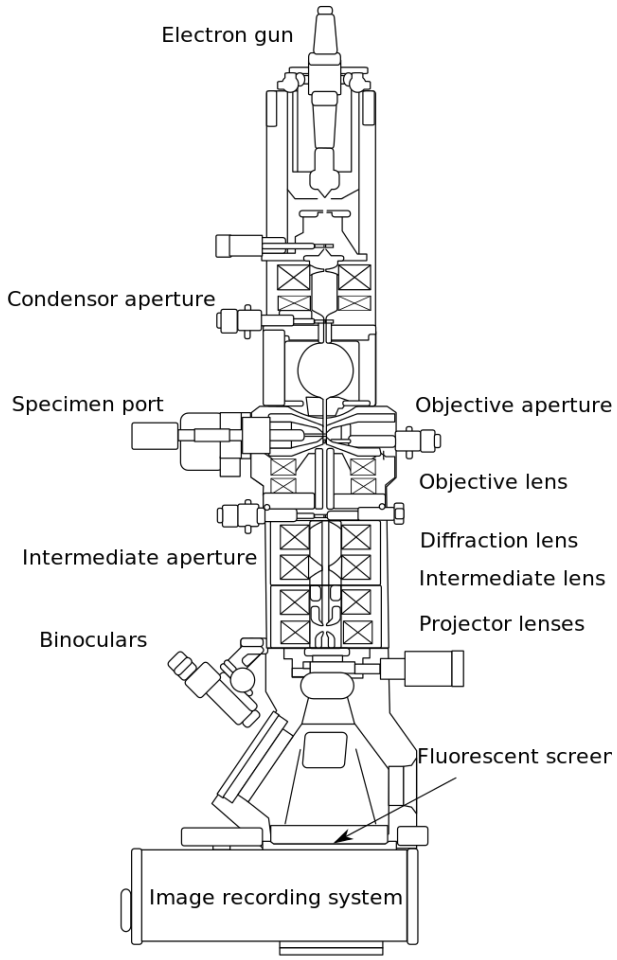

Figure 13: Schematic representation of Transmission Electron Microscopy (TEM) structure [48].

The electron-optical system of TEM (Figure 13) is made of an electron gun which produces the electron beam, and several magnetic lenses. Basically it is possible to distinguish three main sections of the instrument [49]:

- *illumination system*: it includes the electron gun and two or more condenser lenses used to focus electrons onto the sample
- *specimen stage*: it contributes to maintain the mechanical stability of the sample
- *imaging system*: it contains at least three lenses used to produce the magnified image of the sample on a fluorescent screen or on the monitor screen of an electronic camera system.

3.1.2 *Dynamic Light Scattering (DLS)*

Dynamic Light Scattering (DLS) is a *non-invasive technique* also known as Photon Correlation Spectroscopy (PCS) or Quasi-Elastic Light Scattering (QELS). It is a tool used for measuring the size of molecules, nanoparticles and sub-micron colloids.

Basically, DLS measures the Brownian motion of particles induced by the solvent molecules in which they are. The measured velocity of the Brownian motion is defined by the translation diffusion coefficient (D) from which it is possible to evaluate the size of a particle by means the *Stokes-Einstein equation* [50]:

$$d(H) = \frac{kT}{3\pi\eta D} \tag{1}$$

where:

d(H) = hydrodynamic diameter
D = translational diffusion coefficient
k = Boltzmann constant
T = absolute temperature
η = viscosity

In this case the diameter measured by DLS is related to the diffusion of the particle within a fluid, for this reason it is referred to a hydrodynamic diameter. Hydrodynamic diameter is defined as the diameter of a sphere that has the same translation diffusion coefficient as the particle.
Smaller particles are more easily moved by the solvent molecules and so they move more rapidly.
Many factors can affect the result, in particular the nature of the surface as well as the ionic concentration of the medium can change the measure of the size of the particle.

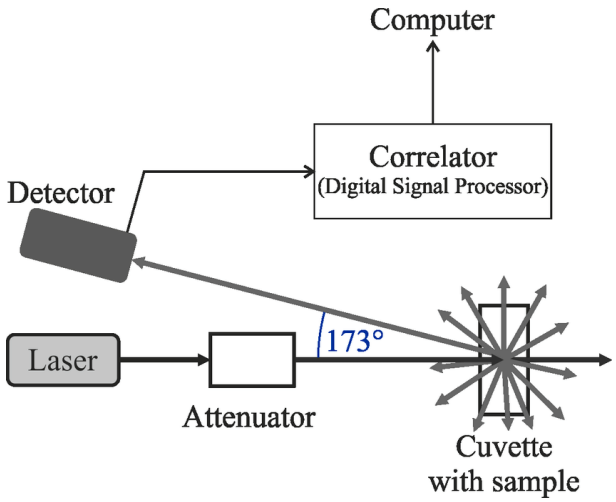

Figure 14: Setup for Dynamic Light Scattering (DLS) of the Malvern Zetasizer Nano ZS [51].

The instrument (Figure 14) comprises a laser that provides the light source to illuminate the sample that has to be small compared to the wavelength of the laser (typically less than $d = \lambda/10$) in order to have scattering of the light (*Reyleigh scattering*). The scattered light is then measured by a detector but in order to avoid the saturation of the detector, an attenuator is used to reduce the intensity of the laser source. After that, the scattering intensity signal is processed by a correlator that is a signal comparator that measures the correlation between two signals or one signal with itself at varying time intervals. Finally, the correlation value is passed to a computer in order to obtain the size by using an algorithm.
There are two approaches that can be used: the first one is known as cumulants analysis for which a single exponential is fitted to the correlation function to obtain the main size (*z-average diameter*) and an estimate of the width of the distribution (*polydispersity index*), the second one fits a multiple exponential to the correlation function to obtain the distribution of particle sizes, such as Non-Negative Least Squares (NNLS) or CONTIN.

3.2 KINETIC STUDIES

The deallylation of a non-fluorescent precursor is a preliminary step required before testing the ability of the nanozymes to activate a prodrug by cleaving the propargyl functionality that has been introduced to block the active side of the original drug [4].
The catalytic properties of both nanozymes (NZs) and polyzymes (PZs) encapsulating iron-porphyrin was analysed.

Kinetic tests were performed by analysing the catalytic potential of nanozymes in carrying out bioorthogonal conversion of a pro-fluorophore into the active form.
In this case the resorufin dye ($C_{12}H_7NO_3$) was chosen since it is highly fluorescent and has a maximum excitation at 563 nm and a maximum emission at 587 nm. The activation of a resorufin-based pro-fluorophore was performed in phosphate-buffered saline (PBS, pH 7.4).

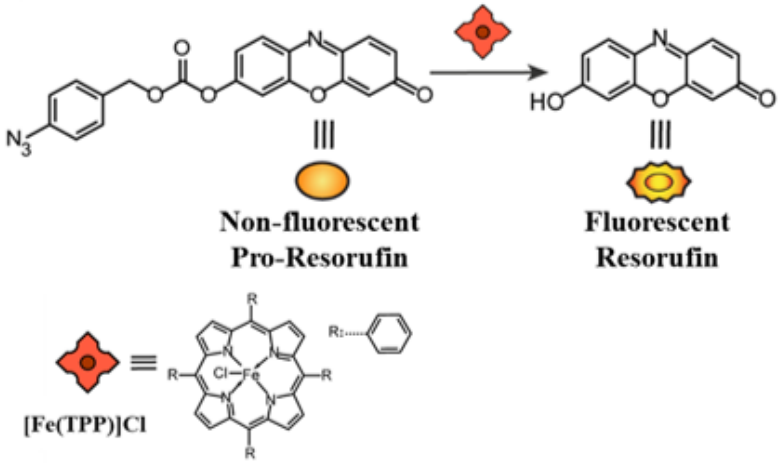

Figure 15: Schematic representation of the activation of aryl-azide protected resorufin by the catalytic behaviour of the iron-porphyrin metal catalyst.

Prof. Rotello and coworkers synthesized the pro-dye (Figure 15) by featuring the resorufin with an aryl azide carbonate unit directly connected to the phenolate of resorufin to let it be non-fluorescent. The catalytic reduction of azide group mediated by [Fe(TPP)]Cl transforms the caging group into a self-immolative linker, releasing the fluorescent resorufin molecule.
The kinetics of NZs and PZs were performed by using a microplate reader (Molecular Device SpectraMax M2) tracking the fluorescence intensity of the dye (Exitation = 570 nm, Emission = 590 nm, Cutoff = 515 nm). Experiments were performed at 25 °C for 2 h until the fluorescence intensity reached saturation.
After that, the temperature was raised to 37 °C in order to study the thermo-responsive behaviour of the nanozymes.

3.2.1 *Catalytic activity of Nanozymes (NZs) in solution*

The catalytic activity of the Au-TTMA and the Au-COOH nanozymes were evaluated by fluorogenic azide reduction of the aromatic azide oxycarbonyl-protected resorufin used as substrate (Figure 16).

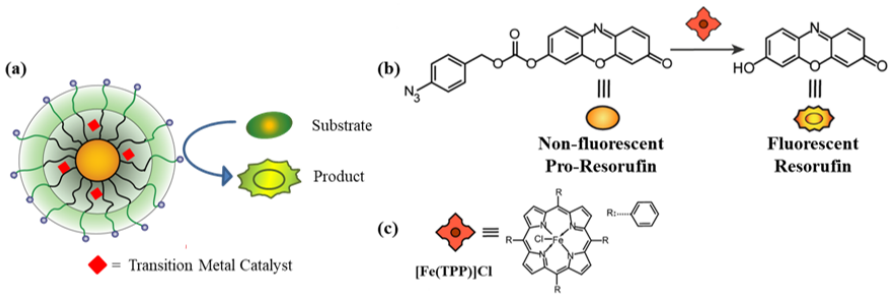

Figure 16: a) Schematic representation of the catalysis mediated by encapsulated Transition Metal Catalyst (TMC), b) Azide reduction reaction catalysed by the catalyst, c) Structure of the iron-porphyrin metal catalyst.

Iron-porphyrin metal catalyst catalyzes the reduction of the azide group to amine, which further triggers the fragmentation of the protecting group.
The catalytic activity of NZs was studied by analysing the activation of the pro-fluorophore. This experiment requires the preparation of 1 mM solution of glutathione (GSH) in PBS. Meggers and co-workers found that in the presence of excess strong thiol nucleophiles (e.g. GSH), the rate-determining step shifts from the allylation step, that is rate-determining, towards the uncaging step. GSH does not affect the reaction rate under biologically relevant conditions, that means that thiol concentrations inside living systems do not decrease the catalytic activity of the catalyst. Instead, nucleophiles enable a fast reaction [52].
The pro-dye was used in two different concentrations, 20 µM and 30 µM respectively, by diluting the stock solution in PBS. In these tests, the catalytic behaviour of three different concentrations of NZs were analysed. According to this requirement, NZs were diluted in PBS to 100 nm, 200 nm and 300 nm respectively.
The preparation of a Costar black 96-well plate was done by adding, in each well, a solution with a volume of 100 µL.
First 10 µL of GSH solution and 10 µL of pro-fluorophore were released in each well. Then, 80 µL of the nanozyme solution was then added quickly in each well, bringing the overall volume in each well to 100 µL. Every nanozyme concentrations were done in triplicates to record the range of responses. For the control groups, 80 µL of PBS was added to the previous dropped GSH and pro-dye.

The catalytic behaviour of both the Au-TTMA and the Au-COOH nanozymes was performed (Figure 17).

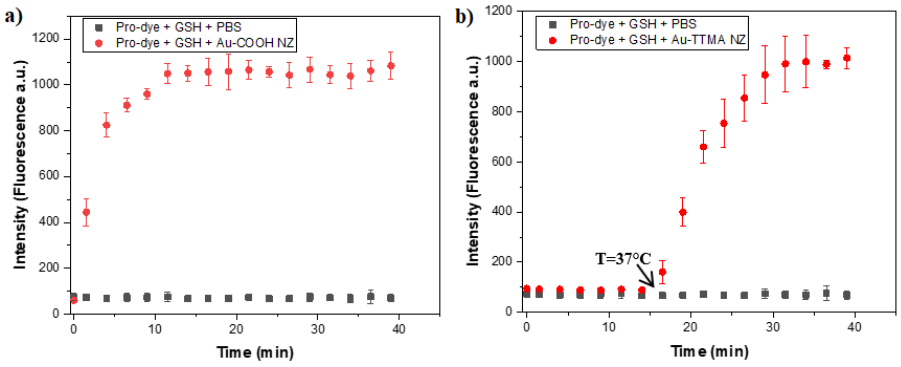

Figure 17: Kinetic trends of the iron-porphyrin encapsulated in (a) Au-COOH, and in (b) Au-TTMA nanozymes.

The Au-COOH NZs were found to catalyze the deprotection of the pro-fluorophore to produce the active fluorophore, resorufin, at 25 °C. While, the Au-TTMA NZs showed thermo-responsive behaviour. Indeed, at 25 °C the NZs did not catalyse the bioorthogonal reaction. This might be due to the steric hindrance caused by the terminal charged moieties, and the stacking of the metal catalyst at lower temperature which prevents the pro-fluorophore to interact with the TMC. When the temperature is raised to 37 °C, the mobility of the ligand chain might increase. Probably, this might lead to the disruption of the stacking amongst the metal catalysts, hence, exposing them to the pro-fluorophore to bring about deprotection of the pro-fluorophore (Figure 18).

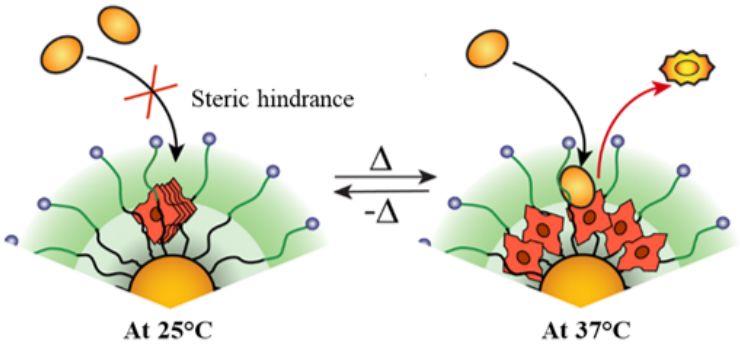

Figure 18: Thermo-responsive catalytic behaviour of the Au-TTMA nanozymes.

Notably, no reaction was observed in the control group where no nanozyme were added. This confirms the ability of the protecting group to quence the fluorescence of the dye.

3.2.2 *Catalytic activity of Polyzymes (PZs) in solution*

The catalytic behaviour of the polyzymes (PZs) was also investigated. To examine their activity, the non-fluorescent pro-fluorophore molecule was used as substrate and was activated to fluorescent molecule (resorufin) in the presence of [Fe(TPP)]Cl catalyst (Figure 19).

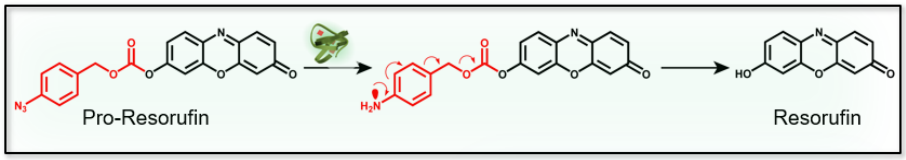

Figure 19: Schematic representation of the activation of the pro-fluorophore mediated by the polyzyme (PZ).

The experiment was run following the same procedure used to evaluate the catalytic activity of the NZs (Section 3.2.1).
In this case the experiment was run at 25 °C only since the thermoresponsive behaviour of the polyzyme is not expected.

As before, each well of a Costar black 96-well plate was prepared by dropping a solution with a volume of 100 µL. First, 10 µL of 1 mM GSH solution prepared in PBS and 10 µL of pro-fluorophore were released in each well. Then, 80 µL of the polyzyme solution previously prepared in PBS was then added quickly bringing the overall volume in each well to 100 µL.
Also in this case, every polyzyme concentrations were done in triplicates to record the range of responses and the control groups were prepared by adding 80 µL of PBS to the previous dropped GSH and pro-dye.
Two different concentrations of pro-fluorophore, 20 µM and 30 µM respectively, were prepared by diluting the stock solution in PBS. In these tests, the catalytic behaviour of three different concentrations of PZs were analysed: 50 nM, 100 nM and 200 nM respectively were diluted in PBS.
The catalytic activity of the PZ is here reported (Figure 20).

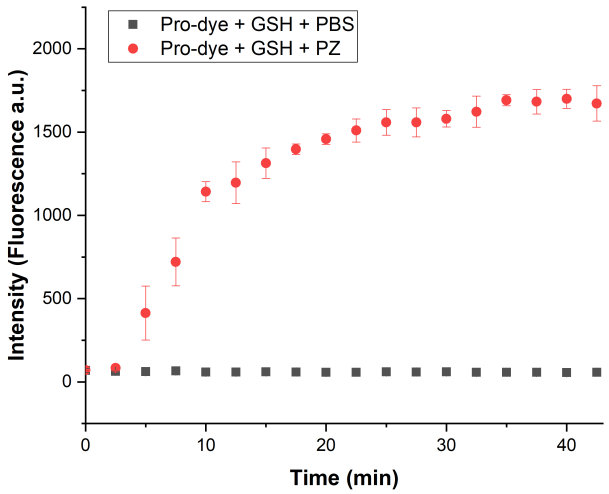

Figure 20: Kinetic trends of the iron-porphyrin encapsulated in the polyzyme (PZ).

It can be noticed that the PZ is able to catalyze the deprotection of the pro-fluorophore to produce the active fluorophore, resorufin. No reaction was observed in the control group where the only aryl-azide protected resorufin was added. This confirms the ability of the protecting group to quence the fluorescence of the dye.
The result shows that the metal catalyst encapsulated into a polymer-based scaffold is able to activate the aryl-azide protected resorufin producing fluorescence. Looking at the Figure 20 it is possible to notice that the catalysis is pretty fast and so the unmasking of the pro-fluorophore is performed in a short time.
The study of the catalytic activity of the PZ in a solution is a preliminary test before testing its catalytic behaviour inside the biofilm.

3.3 SIZE CHARACTERIZATION

Size distributions and dimensions of nanoparticles were analysed by using Dynamic Light Scattering (DLS) and Transmission Electron Microscopy (TEM). First, the gold nanoparticles (AuNPs) and nanozymes (NZs) were studied in order to get the presence of possible aggregations. Second, polymeric nanoparticles (PNPs) and polyzymes (PZs) samples were characterized.

3.3.1 *DLS and TEM characterization of gold nanoparticles (AuNPs) and nanozymes (NZs)*

Hydrodynamic diameter of the nanoparticles and the zeta potential were measured by dropping the desired solution (1 μM) in a cuvette containg PBS. The cuvette was analyzed by using a Malvern Zetasizer Nano ZS instrument. The measurement angle was 173° (backscatter) and data were analysed by the "multiple narrow modes" (high resolution) based on non-negative-least-squares (NNLS).
The sizes and the zeta-potential of the gold nanoparticles (AuNPs) and the nanozymes (NZs) are shown in the Table 2.

Table 2: Size distribution of Au-TTMA and Au-COOH NPs and NZs recorded by DLS.

	DIAMETER (nm)	ζ-POTENTIAL (mV)
Au-TTMA NP	6.121 ± 0.83	$+34 \pm 3.55$
Au-TTMA NZ	5.698 ± 1.25	$+32.1 \pm 1.79$
Au-COOH NP	7.21 ± 1.39	-22.253 ± 1.71
Au-COOH NZ	6.53 ± 0.54	-21.58 ± 0.88

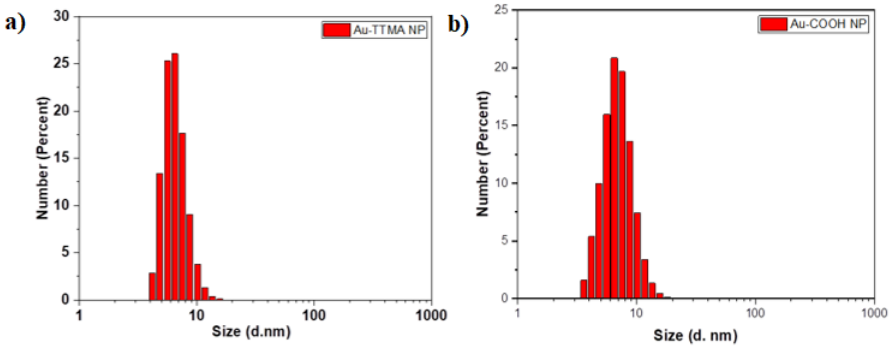

Figure 21: DLS measurements of the a) Au-TTMA and b) Au-COOH nanoparticles.

DLS results (Figure 21) indicate that the AuNPs are not aggregated and they maintain their hydrodynamic radii range even after the encapsulation of the iron-porphyrin metal catalyst (Table 2). As expected, DLS measurements show that the size of NPs after catalyst encapsulation stays same. The $2\,nm$ Au core functionalized with ligands shows an overall size of ~ 10 nm.

The AuNPs were also characterized using Transmission Electron Microscopy (TEM). TEM samples were prepared by placing one drop of

the desired solution (600 nM) onto a 300-mesh Cu grid-coated with carbon film. These samples were analyzed and photographed using JEOL 2000FX electron miroscopy by exploiting an accelerating voltage of 200 kV. The instrument is able to produce magnified images of the sample with high resolution in the range of $10^3 - 10^6$.
The average diameter of Au core before and after encapsulation of iron-porphyrin metal catlysts is ~ 2 nm as expected (Figure 22).

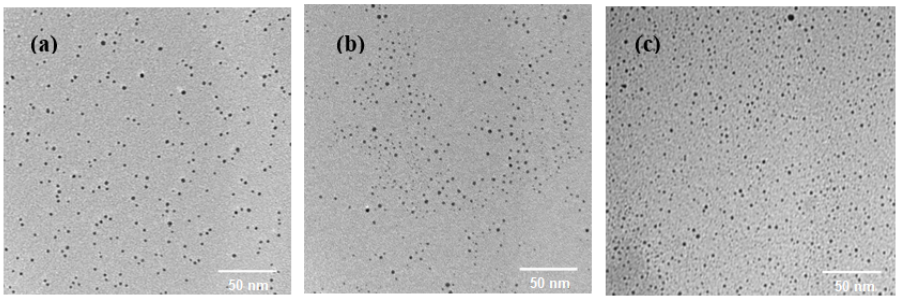

Figure 22: TEM images of the a) Au core, b) Au-TTMA and c) Au-COOH nanoparticles. Scale bars are 50 nm.

3.3.2 *DLS and TEM characterization of polymeric nanoparticles (PNPs) and polyzymes (PZs)*

Polymeric nanoparticles (PNPs) generated by the self-assembling of the polymer $PONI-C_{11}-TMA$ in an aqueous solution were already analysed by Prof. Rotello and coworkers [1]. It was showed that the polymeric nanoparticles present an average size ~ 20 nm as DLS measurement states and this is confirmed by TEM images of polymeric nanoparticles (Figure 23).

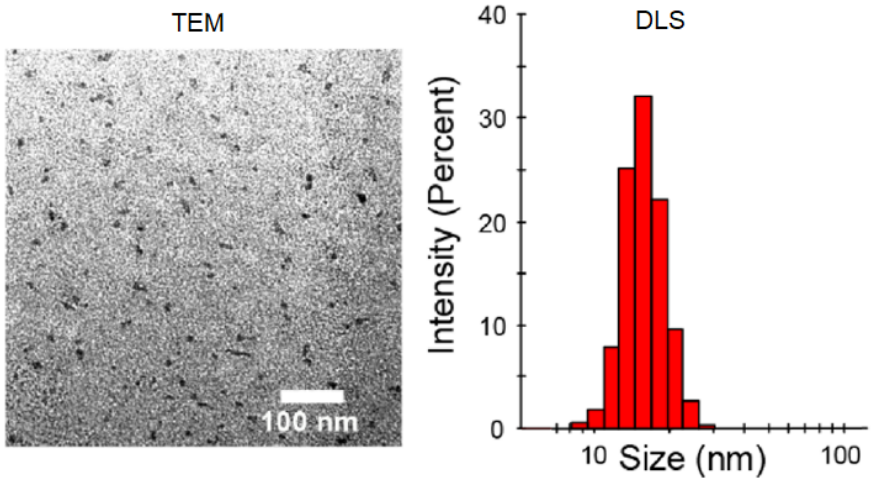

Figure 23: Characterization of $PONI - C_{11} - TMA$ particles using TEM imaging and DLS measurement

Regarding polyzymes (PZs), DLS measurements and TEM images of the polymer-based scaffold encapsulating the iron-porphyrin metal catalyst show an increasing of the size of the nanoparticles (Figure 24). The average diameter of the polyzyme measured by TEM is ~ 35 nm. This is confirmed by DLS data.

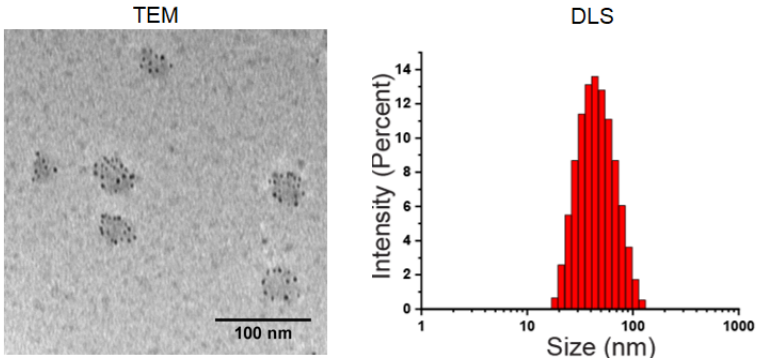

Figure 24: Characterization of polyzymes (PZs) using TEM imaging and DLS measurement.

Also in this case hydrodynamic diameters were measured by dropping the desired solution (1 μM) in a cuvette containg PBS. The cuvette was analyzed by using a Malvern Zetasizer Nano ZS instrument. The measurement angle was 173° (backscatter) and data were analysed by the "multiple narrow modes" (high resolution) based on non-negative-least-squares (NNLS).
Regarding TEM measurements, samples were prepared by placing one drop of the desired solution (10 μM) onto a 300-mesh Cu grid-coated with carbon film. These samples were analyzed and photographed using JEOL 2000FX electron microscopy by exploiting an accelerating voltage of 200 kV, producing magnified images of the sample with high resolution in the range of $10^3 - 10^6$.

Part III

EXPERIMENTAL METHODOLOGY

4

BIOFILM PENETRATION USING POLYZYMES (PZS)

Having characterized the activity of the polyzyme (PZ), testing its catalytic behaviour, the bioorthogonal catalysis performed by this nanocatalyst in biofilms was then probed.
Confocal Laser Scanning Microscopy (CLSM) images were analysed proving the ability of the polyzyme to get inside the biofilm and showing the activation of a non-fluorescent pro-dye to a fluorescent molecule (resorufin) in presence of the iron-porphyrin Fe[TPP]Cl metal catalyst.

The first experiment was performed in order to demonstrate the ability of the polyzyme (PZ) to allow the penetration of the hydrophobic metal catalyst inside the biofilm. Indeed, the PZ is able to create a path in the dense extracellular polymeric substances (EPSs) matrix of the biofilm allowing the iron-porphyrin Fe[TPP]Cl to penetrate inside it.
This feature of the PZ can be exploited for optical imaging of the biofilms; the embedded transition metal catalysts (TMCs) can activate pro-fluorophores *in situ* inside the biofilms. Polyzymes provide an effective imaging system amplifying the fluorescent signal output using bioorthogonal catalysis.
The use of PZs for imaging applications of biofilms were investigated by using Confocal Laser Scanning Microscopy (CLSM) analysing the generation of the fluorophore (resorufin) through the deallylation of a non-fluorescent precursor. To this aim, GFP (Green Fluorescent Protein)-expressing *E. Coli* (CD-2) biofilms were used in order to investigate the co-localization of the activated dye and the biofilm.

4.1 OPTICAL MICROSCOPY

Optical microscopy is a characterization technique that exploits visible light transmitted or reflected from a sample using optical lenses in order to get a magnification of the object. This technique uses photons both as source to excite the specimen and as signal to detect, but it can have different configurations depending on both the sample and the desired results:

- *Bright-field* illumination, in which the contrast of the image is due to the absorbance of the light in the sample

- *Dark-field* illumination, where the contrast is due to the scattered light from the sample
- *Cross-polarized light* illumination, that uses the rotation of polarized light after the interaction with the sample
- *Phase contrast* illumination, that exploits the interference of light coming from different paths
- *Confocal*, that is a scanning technique using a pinhole in order to avoid the out-of-focus light to reach the detector
- Others.

The main limit of this kind of technique is the resolution. Resolution is defined as the shortest distance between two points on the sample that can be distinguished in an optical microscope. The main limitation results to be the diffraction effect, strictly related to the source wavelength. The maximum resolution that can be obtained through an optical microscope is $\sim 0.5\,\mu m$, due to the fact that the visible light wavelength is around $500\,nm$.

4.1.1 *Confocal Laser Scanning Microscopy (CLSM)*

A brief description of the Confocal Laser Scanning Microscopy (CLSM) is here exposed.

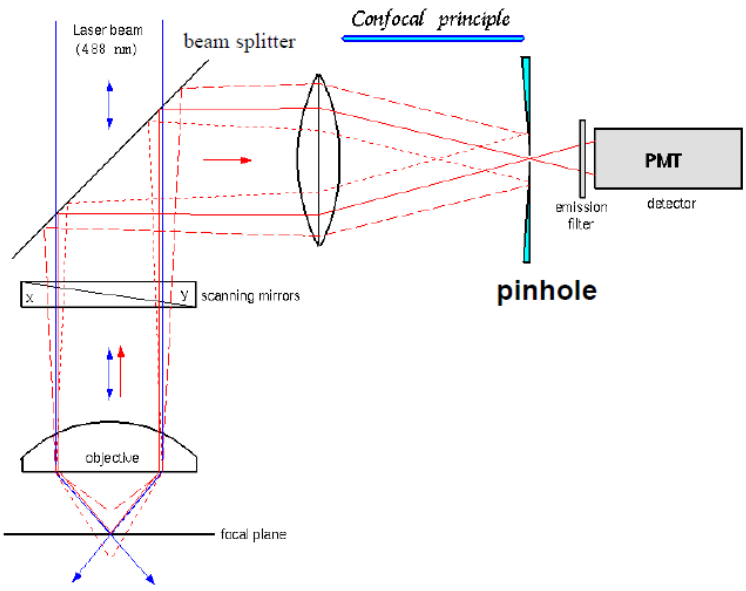

Figure 25: Schematic representation of the Confocal Laser Scanning Microscopy (CLSM) structure [47].

Confocal Laser Scanning Microscopy (CLSM) or Laser Confocal Scanning Microscopy (LCSM) (Figure 25) is an optical imaging technique that exploits the confocal configuration increasing optical resolution and contrast of images with respect to the standard configuration. While the standard microscopy illuminates all the sample by a focused photon beam, the confocal microscopy allows to reconstruct, step by step, for each point of the sample surface, the intensity of the reflected light which is strictly correlated to the morphology of the sample. This allows to obtain a 2D mapping thanks to the raster mapping.

To increase the spatial resolution, confocal configuration exploits a beam that is similar to a sphere of minimum confusion where the sample is excited. This optical sphere has a certain wideness related to the numerical aperture (NA) of the objective lens and so it depends on its focal length and magnification.

The source is a collimated, polarized laser beam that emits a monochromatic beam which is confined as a cylinder. It can be shrinked by the objective lens at the apix of the core on the focal length of the lens. Then, the beam is scattered, diffused, partially reflected by the sample and collected by the same objective lens. It can be deflected stepwise in the x- and y-direction to respect the sample surface by scanning mirror which can change position in order to perform raster scanning pattern so, for each point, the light-sensitive detector (photomultiplier) measures the reflected beam from the sample surface. Indeed, through other lenses, the beam can be focused on the active area of the photodetector which is able to produce a current proportional to the photon flux impinging on its area.

For each single point, a collimated beam of the excitation area of the sample surface is obtained and three different optical paths can be recoiled on the other side of the system. The beam splitter is able to deviate the majority of the light towards another convergent convex lens. Several optical rays will be convergent in different points. In order to reduce this problem, a small pinhole, i.e. the confocal aperture, whose diameter is $\sim 10\,\mu m$, can be used, so one of the optical rays can be intercepted eliminating all the out-of-focus light, i.e. all light coming from regions of the specimen above or below the plane of focus. Therefore, the CLSM does not only provide excellent resolution within the plane of section ($0.25\,\mu m$ in x and y directions), but also yields similarly good resolution between section planes ($0.3\,\mu m$ in z direction).

Moving the objective lens, if the focus length (distance between the objective and the sample) is increased or decreased, different regions at the surface of the sample can be excited and a 3D morphology of the sample can be reconstructed if the sample is partially transparent.

Time scanning depends on the area to magnify and on raster scan-

ning speed.
A maximum magnification of $1000 - 1500$ and the highest spatial resolution of few $100\,nm$ can be reached using visible range. The spatial resolution can be increased decreasing the wavelenght of the laser beam.

4.1.2 *Green Fluorescent Protein (GFP)*

Recently, the green fluorescent protein (GFP) from the jellyfish *Aequorea victoria* [53] has emerged as one of the most interesting proteins that shows a highly visible fluorescence without using fluorophores. The bright green bioluminescence of GFP became a widely genetic tool exploited in biochemistry and cell biology. Thanks to a rigid shell embedding the chromophore in GFP, the fluorescence can be protected by photobleaching [54]. Even though the GFP is the result of introducing a foreign gene into the cell [55], it does not interfere with cell growth and function.

The fluorescent intensity of GFP expressed in living microorganisms introduces an optical label or indicator in several imaging and biological applications. This is a *non-invasive technique* used to investigate structural relationships between organelles, intra and intercellular trafficking of proteins, properties of different mutants and recently, it became an interesting tool for single-molecule spectroscopy [56].
Since the sample can be excited at only one wavelength, without requiring any additional cofactors or substrates, photons emitted by the monochromatic laser of the confocal laser scanning microscopy was used in order to excite the GFP fluorophore.

4.2 IMAGING APPLICATION OF POLYZYMES (PZS)

In this section the penetration of the hydrophobic metal catalyst embedded in the polymer-based scaffold inside the biofilm was analysed. This specific ability is an important strategy that can be exploited for biofilm imaging.
The experiment procedure is the same one performed in the Section 3.2, here repeated but in different conditions: in this case the pro-fluorophore activation is not done in solution but inside the biofilm. Confocal images confirm that the catalytic activation of the pro-dye into a fluorescent molecule (resorufin) happens inside the biofilm thanks to the encapsulated iron-porphyrin Fe[TPP]Cl inside the polymeric-scaffold.
The deallylation of a non-fluorescent precursor inside the biofilm is a preliminary step required before testing the ability of the polyzymes

to activate a pro-drug by cleaving the propargyl functionality that has been introduced to block the active side of the original drug [4].

4.2.1 *Biofilm GFP-expressing E. Coli culture*

In this project, *Escherichia Coli* (*E. Coli*, CD-2)-expressing GFP (Green Fluorescent Protein) has been treated in order to investigate the penetration of the TMC inside the biofilm thanks to the polymeric shielding by monitoring the fluorescence intensity of the resorufin after the deallylation of the pro-fluorophore.
The reaction is the one analysed in the Section 3.2. The deprotection of the pro-dye is here analysed inside the biofilm verifying the biofilm penetration ability of the PZ.

E. Coli (CD-2) bacteria were cultered in Lysogeny Broth (LB) medium at 37 °C and 275 rpm until stationary phase overnight. The cultures were then harvested by centrifugation and washed with 0.85 % sodium chloride (NaCl) solution for three times.
After that, the optical density (OD) has been measured at 600 nm in order to determine the concentration of resuspended bacterial solution. Once the OD of bacteria was known, M9 solution was used to dilute bacterial solution to a concentration of $1x10^8$ bacterial cells/mL.
The green fluorescent protein production was induced by adding 1 µM of isopropyl-β-d-thiogalactoside (IPTG) to the bacterial solution.
Confocal dishes were prepared by adding in each well 3 mL of the bacterial solution. After that, they were covered with aluminum foil in order to prevent any photobleaching of the fluorescence generated by the GFP.
Bacteria were incubated at room temperature under static conditions allowing the bacteria growth and proliferation and the old medium was replaced every 24 h. After three days, GFP-expressing *E. Coli* (CD-2) biofilms grew and the medium was replaced by 100 nM of the polyzyme solution. The incubation of the biofilms with the PZs was done for 2 h.
Two control groups were prepared: one is obtained by incubating the biofilms with only M9 media in order to verify that there is no contamination of the media and that the biofilm can grow without any problems, while the other sample was prepared by replacing the medium with the only substrate in order to demonstrate that the pro-dye is not able to be self-activated but instead it requires the presence of the metal catalyst.
After 2 h, biofilms incubated with PZs were washed three times using PBS to remove any polyzyme from the surface of the biofilm and were incubated with a fresh media containing the substrate for 2 h.
Before analyzing the samples with the confocal microscopy, all sam-

ples were finally washed again three times using PBS.
A schematic representation of confocal dish samples is shown in Figure 26: two samples were used as control groups to be sure that there is no activation of the pro-fluorophore in absence of the polyzymes.

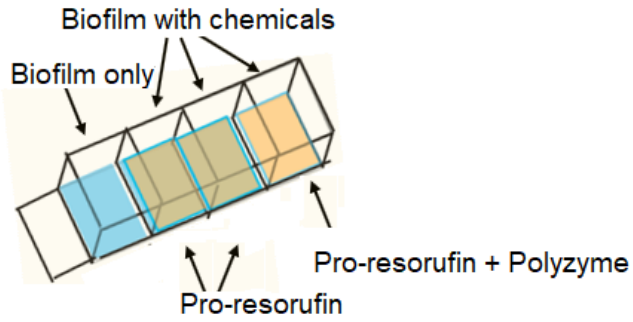

Figure 26: Schematic illustration of the confocal microscopy experiment setup.

4.2.2 *Confocal Imaging of biofilms*

Confocal microscopy images were obtained on a Nikon A1 spectral detector confocal microscope (A1SP) using a 60x objective. Viable GFP-expressing *E. Coli* biofilms emit green fluorescence at 515 nm λ_{em} and should be excited at 490 nm λ_{ex}. The activated resorufin emits red fluorescence should be excited at 570 nm λ_{ex} and emits at 590 nm λ_{em}. The settings of the confocal microscope were done according to that.
Confocal microscopy images are here shown (Figure 27).

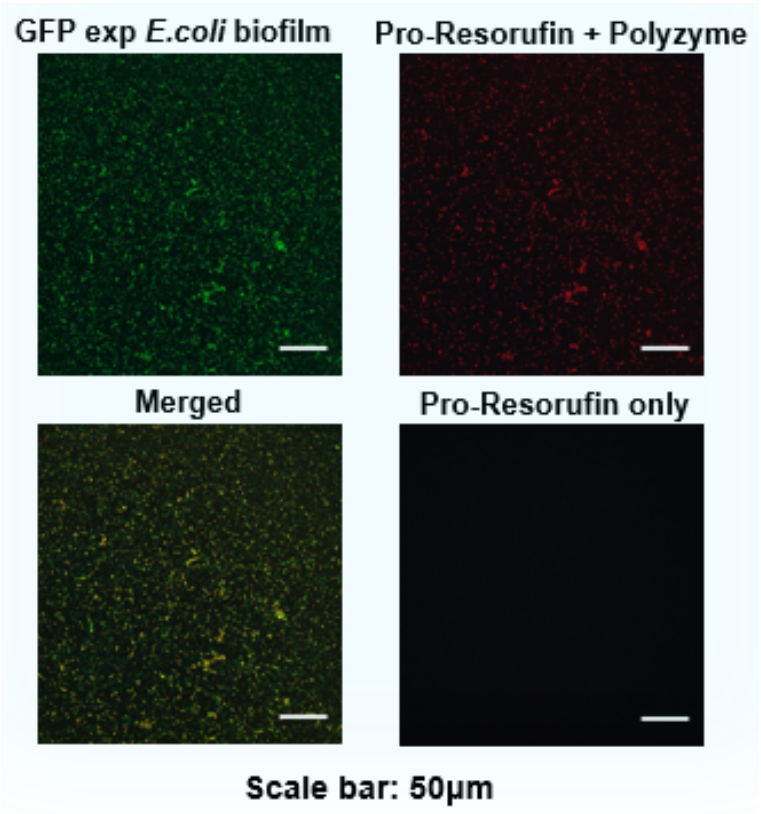

Figure 27: Confocal microscopy images show successful *in vitro* activation. **I.** GFP (green fluorescent protein)-expressing *E. Coli* (CD-2) biofilms. **II.** Red fluorescence of activated resorufin. **III.** Merged of I and II. **IV.** Pro-resorufin only as control group. Scale bars are 50 µm.

Biofilms incubated with only the pro-fluorophores were used as negative control demonstrating that the pro-dye alone was not activated in absence of the iron-porphyrin metal catalyst.
Confocal microscopy images (Figure 27) show that biofilms treated with PZs have bright fluorescence. This means that the PZ is able to penetrate the biofilm creating a path in the dense EPS barrier and to perform catalysis inside it. The deprotection of the pro-fluorophore turned into a fluorescent molecule is shown by the red fluorescence of the resorufin activated by the metal catalyst inside the biofilm.
The green biofluorescence of the GFP (green fluorescent protein)-expressing *E. Coli* (CD-2) biofilms was exploited in order to further demonstrate the co-localization of the activated pro-resorufin and the biofilm: the resulting merged demonstrates that the activation of the pro-dye happened only inside the biofilm mediated by the nanocatalyst.

Confocal microscopy is a useful tool for investigating the ability of the polyzyme to penetrate the EPS matrix of the biofilms. This may be a promising strategy for a rapid and effective imaging of biofilms: the PZs can penetrate the EPS matrix of the biofilm and the bioorthogonal catalysis provides a sensitive readout mechanism. This strategy can be also exploited for therapeutic applications: penetrated and accumulated inhibited antibiotics inside biofilms can be activated by bioorthogonal catalysis.

5

BIOORTHOGONAL CATALYSIS IN BIOFILMS

Having established the ability of the polyzyme (PZ) to penetrate the biofilm and verified that the bioorthogonal catalysis can be performed inside the biofilm, the pro-drug activation catalysed by the Transition Metal Catalyst (TMC) encapsulated in the polymer-based scaffold were carried out proving the therapeutic application of the designed nanocatalyst.
The therapeutic ability of the nanocatalyst against preformed bacterial biofilms was quantified. The penetration of the PZ inside the biofilm, as proved by confocal images, can be therefore exploited in therapeutic applications. Indeed, the encapsulated iron-porphyrin metal catalyst can be used to catalyse the activation of a pro-drug turning it into an antimicrobial agent.
In this project the fluoroquinolone Moxifloxacin were studied and the ability of the polyzyme to eradicate biofilms were investigated.

5.1 ANTIMICROBIAL ACTIVITY STUDIES

This section is focused on the study of antimicrobial efforts on highly refractory biofilms where traditional antibiotic treatments are not very efficient. A quantitative analysis of therapeutic efficacy of polyzymes (PZs) towards enclosed pathogenic bacteria was investigated. The Gram-negative planktonic bacteria *Escherichia Coli* (*E. Coli*) (CD-2) has been taken into account.

The pathogenic *E. Coli* produces lethal toxins causing food poisoning, sepsis, meningitis or urinary tract infections in humans. This uropathogenic bacterium is resistant to many antibiotics used for the treatment of the desease [57]. For this reason the studies were carried out on the *E. Coli* strain CD-2 in order to find an alternative way, with respect to the use of drugs, to treat antibiotic resistant bacteria.

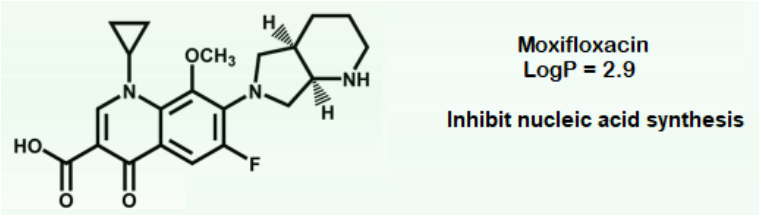

Figure 28: Selected antibiotic: Moxifloxacin (log(P)= 2.9).

In this project, the Moxifloxacin (Figure 28) was chosen because this drug is able of binding to the allosteric sites of DNA gyrase and topoisomerase IV. Therefore, Moxifloxacin functions as an inhibitor of nucleic acid synthesis [58]. The fluoroquinolone Moxifloxacin was also chosen because of its hydrophobicity represented by log(P).The choice is based on the psycochemical properties of the drug such as *lipophilicity*, as the ability of a molecule to interact with an oil phase, and *hydrophobicity*, as the ability to interact with the water [59]. Both of them are commonly measured by the log(P) value: the partition coefficient, abbreviated P, is defined as a particular ratio of the concentrations of a solute between two phases, and the logarithm of this ratio is thus log(P) [60]:

$$\log(P)_{oct/wat} = \log\left(\frac{[solute]^{un\text{-}ionized}_{octanol}}{[solute]^{un\text{-}ionized}_{water}}\right) \tag{2}$$

Pro-drug should be hydrophobic enough to ensure high affinity to the catalyst in the hydrophobic pocket of the polyzyme but not too high hydrophobic, which will render the molecule insoluble.

Prof. Rotello and coworkers synthesized the pro-Moxifloxacin: the fluoroquinolone was converted into a pro-drug via functionalization on its secondary amino group. The modification at this site blocks the binding to the two target enzymes. A bulky aryl-azide carbamate moiety was introduced as a caging group to turn Moxifloxacin into a pro-drug reducing its antimicrobial activity. The synthesized pro-drug (Figure 29) results to be hydrophobic enough to ensure high affinity to the catalyst encapusalated in the PZ and so it is more insoluble than the drug.

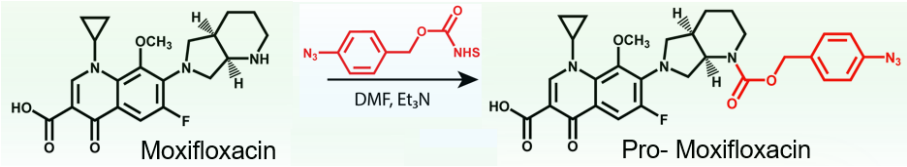

Figure 29: Synthesis of the pro-Moxifloxacin

Before testing the ability of the PZ to perform bioorthogonal catalysis into the biofilm and activate a pro-drug into an antibacterial agent, toxity studies were carried out. These studies allow to know the specific amount of agents that is able to inhibit the growth of the biofilm and to kill the biofilm itself.
Specifically, first the MBIC (Minimum Biofilm Inhibitory Concentration) and then the MBEC (Minimum Biofilm Eradication Concentration) were performed.

The MBIC and MBEC determination helps to individuate the "*therapeutic window*" defined as the range of values where the pro-drug is not toxic whereas the drug is.
The antimicrobial studies proved that the toxicity of the drug is drammatically reduced after the introduction of the masking group. This is really helpful for the pro-drug activation experiment where the injection of the non-toxic pro-drug does not kill the biofilm but it is turned into a toxic drug by the catalysis performed by the polyzyme.

5.1.1 *MBIC (Minimum Biofilm Inhibitory Concentration)*

The MBIC (Minimum Biofilm Inhibitory Concentration) is defined as the lowest concentration of an antimicrobial agent, usually a drug, that prevents the visible growth of biofilm bacteria. MBICs are used in antimicrobial susceptibility testing to evaluate the antibacterial efficacy of compounds. These tests measure the effect of decreasing concentrations of chemicals under test over a specific period in terms of inhibition of biofilm growth. MBIC tests are really useful to determine the appropriate concentration required in the final product of the drug [61].
The determination of the MBIC requires the preparation of chemicals first. In this case, the antimicrobial activity of the polyzyme, Moxifloxacin and the pro-Moxifloxacin were evaluated.

E. Coli (CD-2) bacteria were cultered in Tryptic Soy Broth (TSB) medium at 37 °C and 275 rpm until stationary phase. After 2 h, bacteria grew and all planktonic bacteria solutions were collected into a basin and used to grow biofilms: 150 µL of the bacteria solution was then dropped in each well of a 96-well plate.
Biofilms were grown on the pegs on the lid that are dipped in the solution (Figure 30) at 37 °C and 50 rpm until stationary phase for around 5 h. After this period, biofilms were washed using PBS two times maintining the biofilms immersed in the solution for 30 s.

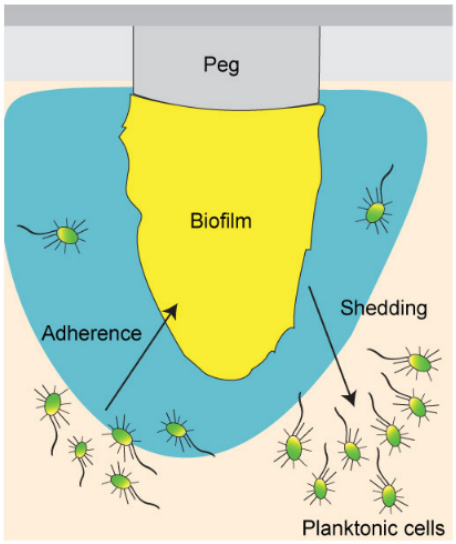

Figure 30: Schematic representation of MBIC/MBEC assay [62].

The lid is then transferred to another 96-well plate prepared in the following way: a volume of 150 µL of M9 media was added in each well and mixed with 50 µL of chemicals in M9 media.
In order to get the MBIC of the specific agent, the concentration of chemicals has to scan a wide range of value. For this reason different concentrations were prepared decreasing the initial stock concentration by half and so on.
The polyzyme was prepared by dissolving the nanocatalyst solution in M9 medium in order to get the starting concentration of 5 µM for MBIC. Starting from this value of the polyzyme, the MBIC was performed by half its concentration well by well spacing in the range $[5 : 0.039063]$ µM.
Moxifloxacin and pro-Moxifloxacin powders were dissolved in 5 % dimethyl sulfoxide ($(CH_3)_2SO$ DMSO). The amount of DMSO used to dissolve agents can not exceed that percentage of the final solution because it could be itself toxic for bacteria. After that, the prepared solution was diluted in M9 media to a concentration of 20 µM for both drug and pro-drug.
This is the starting concentration used in the MBIC procedure that is then decreased by half at each step. The antimicrobial activity of Moxifloxacin and pro-Moxifloxacin was analysed for concentrations within the range $[20 : 0.00061]$ µM.
The growth control group was taken into account adding to few wells only 50 µL of M9 media in order to be sure that the M9 media does not have any contaminations. Every concentration was performed in triplicates in order to get the average of values reducing the error probability of the experiment. In order to reduce risks of contaminations, wells on the border of the plate were not taken into account.

The incubation of bacteria with agents was carried out in an incubator at 37 °C for 22 h.
The optical density (OD) has been measured at 600 nm in order to determine the concentration of resuspended bacterial solution. The reading was done by using a microplate reader (Molecular Device SpectraMax M2) which gives the concentration of the agent that inhibits the biofilm growth.

Table 3: MBIC values evaluated for the polyzyme, Moxifloxacin and pro-Moxifloxacin.

	MBIC (μm)
Polyzyme	0.5
Moxifloxacin	0.002
pro-Moxifloxacin	2

5.1.2 *MBEC (Minimum Biofilm Eradication Concentration)*

The MBEC (Minimum Biofilm Eradication Concentration) is defined as the lowest concentration of an antibacterial agent that results the microbial death over a fixed period under specific conditions. In particular, MBECs indicate the minimum concentration of a chemical that reduces the viability of the initial biofilm by a reduction $\geqslant$ 99.9 % [63].
The MBEC is complementary to MBIC; while the MBIC allows to find the minimum concentration of antimicrobial agent that greatly inhibits growth, the MBEC identifies the minimum concentration of antimicrobial agent resulting in microbial death [61]. This means that, if the MBIC shows inhibition, harvasting bacteria with media might still result in organism proliferation because that MBIC value does not imply microbial death.
Antibacterial agents with the MBEC no more than four time the MBIC can be regarded as bactericidal.
The determination of the MBEC is subsequent to the MBIC test. It can be determinated from the biofilm of MBIC tests by subculturing it with fresh M9 media that does not contain the test agent.

After the washing procedure, when the biofilms were immersed in PBS two times for 30 s, the MBEC experiment can be performed. Biofilms were incubated with 200 μL of M9 media dropped in each well. The incubation were performed in an incubator at 37 °C for 22 h. After the incubation period, the optical density (OD) has been measured at 600 nm in order to determine the concentration of resuspended bacterial solution. The reading was done by using a microplate

reader (Molecular Device SpectraMax M2) which gives the concentration of the agent that kills the biofilm.

Table 4: MBIC and MBEC values evaluated for the polyzyme, Moxifloxacin and pro-Moxifloxacin.

	MBIC (μm)	MBEC (μm)
Polyzyme	0.5	1
Moxifloxacin	0.002	0.03
pro-Moxifloxacin	2	10

For a better interpretetation of results, the biofilm viability test through MBEC is plotted by expressing the concentration of the agent in logarithmic scale (Figure 31).

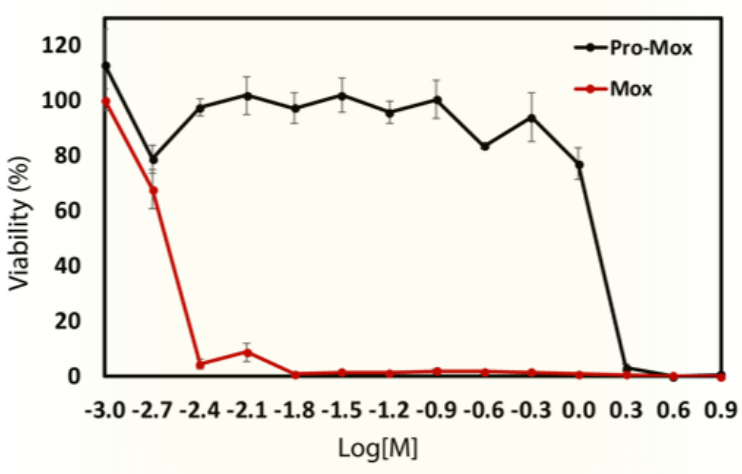

Figure 31: Biofilm viability test through MBEC (Minimum Biofilm Eradication Concentration) in logarithmic scale. Error bars represent standard deviation.

Looking at the Figure 31, it is possible to notice that there is a wide range of values where the pro-Moxifloxacin have no toxicity whereas the Moxifloxacin is able to eradicate the biofilm, that is the so-called "*therapeutic window*". In particular, the conversion of the Moxifloxacin into the pro-drug reduce its antimicrobial activity by more than two orders of magnitude.

5.2 ANTIMICROBIAL ACTIVITY THROUGH PRO-DRUG ACTIVATION USING POLYZYMES (PZS)

Having proved the ability of the polyzyme to get inside the biofilm and to activate the pro-fluorophore, the pro-drug activation can be now performed. After antimicrobial tests it is possible to know approximatively the range where the pro-drug is not toxic whereas the drug is, the so called "*therapeutic window*".
The pro-Moxifloxacin can be turned into the antimicrobial Moxifloxacin by the catalysis performed by the polyzyme. The masking group that inhibits the antibacterial activity of the Moxifloxacin is uncaged by the iron-porphyrin metal catalyst encapsulated in the polymer-scaffold (Figure 32).

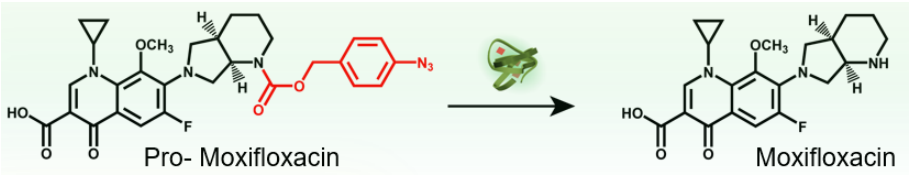

Figure 32: Schematic representation of the activation of pro-Moxifloxacin by using the polyzyme.

The activation of the pro-Moxifloxacin using the polyzyme was performed on the uropathogenic *E. Coli* (CD-2) bacteria and the biofilm viability was determined using Alamar Blue assays according to manifacture's protocol (Invitrogen Biosource).

5.2.1 *Alamar Blue Assay*

The Alamar Blue assay is a method used as an indicator of the proliferation of bacteria and it is also used to study the antimicrobial activity of new agents. Alamar blue contains a specific REDOX indicator that has both fluorescence and colorimetric change relative to the *oxidation-reduction* due to cellular metabolic activity. The change is clear and distinct, so it is easy to be interpreted.
The active ingredient of alamar blue reagent is resazurin ($C_{12}H_7NO_4$): it is a not toxic fluorescent indicator dye and it is easy to be used since it is water soluble.
The bioassay is a powerful tool to understand if the microorganisms is living or not. The growth of the living microorganism under test causes a chemical reduction of resazurin due to the metabolic activity changing the REDOX indicator from oxidized (fluorescent, blue) form to the reduced (highly fluorescent, red) one, resorufin ($C_{12}H_7NO_3$). While, the inhibition of the growth does not lead to any change in the REDOX indicator that maintains the oxidized form [64]. Therefore, just looking at the color of the REDOX indicator, it is simple and easy

to understand which microorganisms are living and which are not. For a further analysis, a microplate reader can be used in order to get specific values indicating the viability of microorganisms.

5.2.2 *Biofilm E. Coli (CD-2) culture*

In this project the uropathogenic *E. Coli* (CD-2) was taken into account in order to study the antimicrobial activity of the Moxifloxacin on this specific bacteria.
This specific drug is able of binding to the allosteric sites of DNA gyrase and topoisomerase IV acting as an inhibitor of nucleic acid synthesis [58].
E. Coli (CD-2) bacteria were cultered in Lysogeny Broth (LB) medium at $37\,^{\circ}C$ and 275 *rpm* until stationary phase overnight. The cultures were then harvested by centrifugation and washed with 0.85 % sodium chloride (NaCl) solution for three times. After that, the optical density (OD) has been measured at $600\,nm$ in order to determine the concentration of resuspended bacterial solution. Once the OD of bacteria was known, M9 media was used to dilute bacterial solution to a concentration of $1x10^8$ bacterial $cells/mL$.
A 96-well plate was prepared by adding $100\,\mu L$ of the bacterial solution in each well. Biofilm were grown in M9 media at room temperature overnight. After this period, biofilms were washed three times using PBS in order to remove resuspended planktonic bacteria.

5.2.3 *Biofilm Viability studies*

E. Coli (CD-2) biofilms were incubated for $2\,h$ with polyzyme at a concentration of $100\,nM$ diluted in M9 media. The plate was wrapped with aluminium foil because of the photosensitivity of the polyzyme and the incubation was done at room temperature. Subsequently, biofilms were washed multiple times using PBS in order to remove polyzymes.
Moxifloxacin and pro-Moxifloxacin powders were dissolved in 5 % DMSO. The amount of DMSO used to dissolve agents can not exceed that percentage of the final solution because it could be toxic for bacteria. After that, the prepared solution was diluted in M9 media to the stock concentration.
Biofilms were incubated with different concentrations of pro-Moxifloxacin ($0, 2.5, 5, 7.5$ and $10\,\mu M$) while some of the biofilms were treated with pro-Moxifloxacin only, Moxifloxacin only and with a combination of pro-Moxifloxacin and polymers as control groups.
The growth control group was taken into account adding to biofilms only M9 media while the sterile control group was realised in order to be sure that the M9 media does not have any contaminations. Each experiment was performed in triplicates in order to get the average

of values reducing the error probability of the experiment.
After the incubation period, 6 h, biofilms were washed again using PBS and the viability of biofilms were determined using Alamar Blue assay.
A solution made of 10 % of alamar blue and 90 % of PBS was prepared and added to each well with a concentration of 100 µL. This procedure was performed turning off the light in order to not change the fluorescence emission of the indicator since the compound is photosensitive.
After that, the plate was incubated in the dark at 37 °C for about 30 min.
The period of incubation depends on the time of reduction of the resazurin in resorufin; the change of the colour from blue to pink/red is clear and distinct so it can be easly noticed by naked eyes.
The viability of *E. Coli* (CD-2) biofilms can be quantitatively measured by using a microplate reader (Molecular Device SpectraMax M2) tracking the fluorescence intensity of the alamar blue indicator (Exitation = 570 nm, Emission = 590 nm, Cutoff = 515 nm). Experiments were performed at 37 °C.

As expected (Figure 33), the pro-drug alone did not show toxicity at any concentration. That confirms the efficiency of masking the antimicrobial activity of the drug after the design. Similarly, the combination of pro-drug and the polymer treatment was not toxic, indicating that the pro-drug activation was mediated by the catalyst loaded in the polymer rather than the polymer itself. However, biofilms treated with pro-Moxifloxacin and polyzyme exhibited a significant decreasing of the viability.

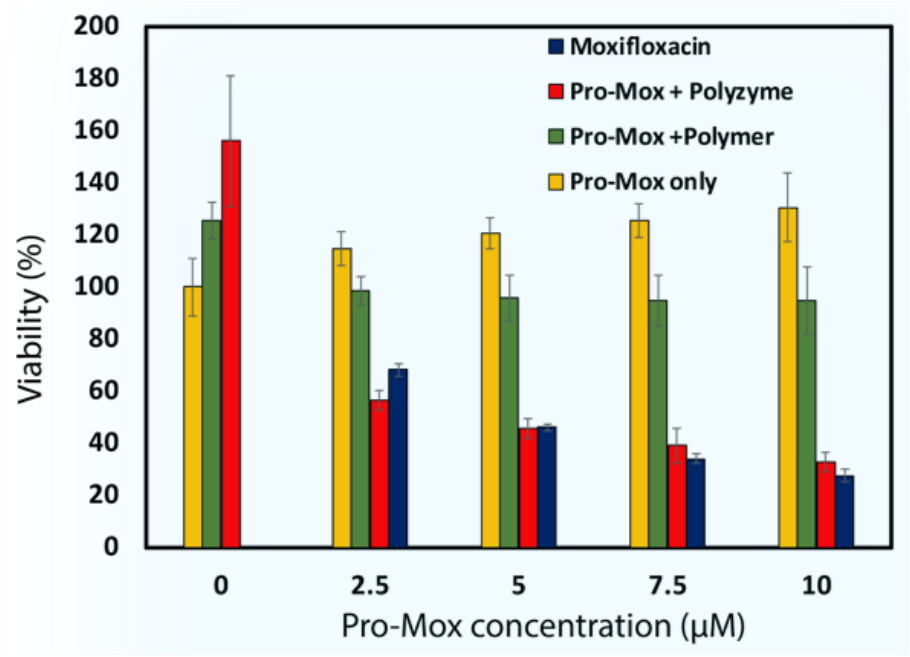

Figure 33: Biofilms treated with pro-Moxifloxacin (yellow bars), Moxifloxacin (blue bars), pro-Moxifloxacin + polymers (green bars) and pro-Moxifloxacin + polyzymes (red bars). Error bars represent standard deviation.

These results show that the polyzyme can activate pro-drugs efficiently for biofilm eradication.
From an antimicrobial perspective, polymer-based nanocatalysts represent a powerful strategy as they can be designed to localize inside the biofilm, reducing side-effects to mammalian tissues, organs and beneficial microorganisms.
Exploiting the ability of the quaternary ammonium polymer ($PONI-C_{11}-TMA$) to penetrate the biofilm, hydrophobic metal catalysts can easily get inside the EPS matrix performing bioorthogonal catalysis inside the biofilm activating pro-drug.
From these preliminary results, it is demonstrated that a cationic polymer facilitates the penetration of TMCs into biofilms and that the efficient pro-drug activation via bioorthogonal catalysis was observed *in vitro*.

Part IV

RESULTS AND DISCUSSION

6 RESULTS AND OUTLOOK

In this project the ability of the polymeric scaffold to allow the penetration of the hydrophobic TMCs inside the biofilm is successfully shown. The fabricated polyzymes (PZs) efficiently catalyze the formation of an active fluorophore and/or drug under physiological conditions.
Having proved the ability of a cationic polymer to create a path through the EPS matrix of the biofilm for the hydrophobic TMC and to activate a pro-drug through bioorthogonal catalysis inside the biofilm, the research can be carried on proposing the achievement of two main aims.
This chapter is therefore dedicated to introduce further studies that can be aimed to improve this strategy. The good results obtained in this project can be a starting point for a wide range of applications. For this reason some optimizations for this work are here proposed: the first aim regards the engineering of the polymer surface to achieve biofilm targeting ability minimizing side-effects, so the functionalization of the polymer-based nanocatalyst is here presented, while, the second one is proposed in order to pursue a combination therapy via multidrug activation to achieve enhanced therapeutic efficacy and expanded antimicrobial spectrum.

6.1 MINIMIZE SIDE-EFFECTS BY DESIGNING A BIOFILM-TARGETING POLYZYME (PZ)

The therapeutic efficacy of the polyzyme (PZ) can be greatly enhanced functionalizing the polymer surface in order to specifically target the biofilm.
Biofilm targeting is a crucial feature in theranostic for therapeutic efficacy.
Technologies for biofilm targeting can follow two main approaches [65]:

- physical-mechanical action, removing the biofilm
- surface coating or eluting substrates used for biofilm prevention.

Targeting the dense EPS matrix can be an interesting strategy to eradicate biofilms that can be obtained by disrupting the EPS matrix or by inhibiting the production of it.
Biofilm micro-environments are inherently acidic as a result of sugar

fermentation caused by bacteria (pH 4.5–6.5) [66]. The pH difference between normal tissue (pH 7.2–7.4) and biofilm EPS matrix represents a promising strategy for selective accumulation of the PZ into the biofilm for both therapeutic and imaging applications.

In a previous work [19], Prof. Rotello and coworkers designed a pH-switchable gold nanoparticle for biofilm targeting. Based on these results, it is possible to synthesize a polymer featured with pH-responsive sulfonamide functional groups that can be used to encapsulate the transition metal catalysts creating a pH-switchable polyzyme. This specific functionalization of the polymer surface can be used to target the acidic environment that characterizes the biofilm bacteria [67]. In this strategy, the biofilm-targeting ability of the polymer is achieved by changing the surface charge at different pH values. Targeting of the biofilm can be achieved through charge-switchable polyzyme (Figure 34) that can have a transition from *zwitterionic* (non-adhesive) to *cationic* (adhesive) at the pH values typically found in the acidic environment of biofilms [19].

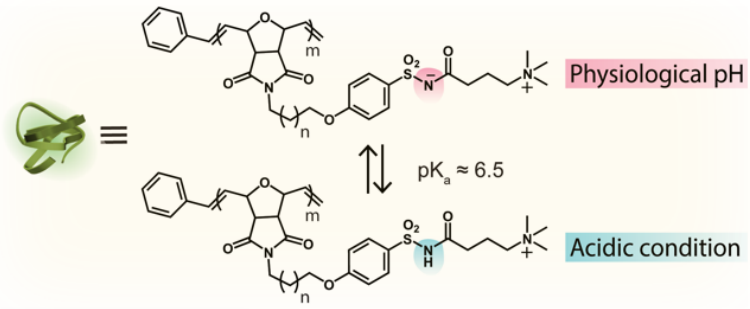

Figure 34: Schematic representation of the pH-responsive polymers (zwitterionic and cationic).

This specific feature of the polyzyme allows to have a broad-spectrum recognition platform for bacteria with selectivity towards biofilm with respect to healthy mammalian cells.
This pH-dependent zwitterionic-to-cationic charge conversion system could be a great candidate as scaffold for therapeutic applications. Basically, the designed zwitterionic polymeric nanoparticle has a low cellular uptake in a neutral pH environment. When the pH of the environment becomes more acidic, as in the case of biofilms, the zwitterionic group becomes cationic enhancing the cellular uptake (Figure 35) [67].

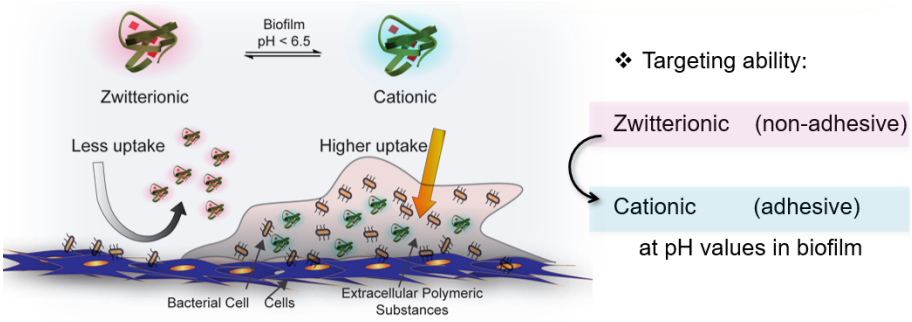

Figure 35: Schematic representation of the selective targeting of biofilm infections using pH-responsive polyzymes.

6.1.1 *Fabrication and characterization of pH-responsive polyzyme (PZ)*

The synthesis of the pH-responsive polymer can be easily obtained by the functionalization of the starting polymer (Section 2.2.1) used in the previous studies (Figure 36).

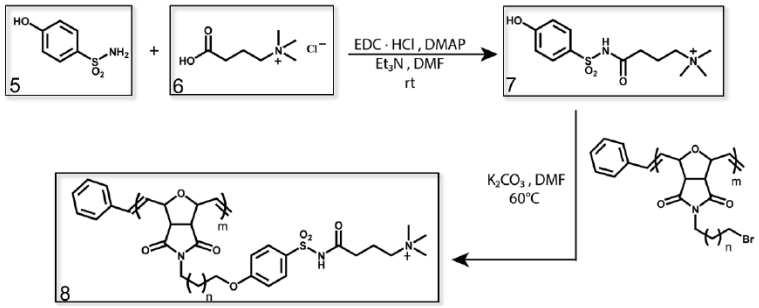

Figure 36: Synthesis of the pH-responsive polymer.

The terminal functional group of the pH-responsive polymer **7** will be synthesized through amide coupling using 4-hydroxybenzenesulfonamide ($C_6H_7NO_3S$) **5** and (3-carboxypropyl)-trimethylammonium chloride ($C_7H_{16}NO_2Cl$) **6**. To this solution, 4-dimethylaminopyridine ($C_7H_{10}N_2$, DMAP) and triethylamine ($C_6H_{15}N$, Et_3N) in dimethylformamide (C_3H_7NO, DMF) and N-Ethyl-N'-(3-dimethylaminopropyl)carbodimide hydrochloride ($C_8H_{17}N_3$·HCl, EDC·HCl) are added.
Once the desired ligand is obtained, the previously used polymer will be post-functionalized with a pH-responsive functional group obtaining the final polymer structure **8**.
The fabrication of the charge-switchable polyzyme can be carried out by encapsulating the [Fe(TPP)]Cl catalyst into the pH-responsive polymeric scaffold. The same procedure previously used for the fabrication of the cationic polyzyme (Section 2.2) is here exploited obtaining the encapsulation of the iron-pophyrin metal catalyst into the hydrophobic pocket.

The same tools used to characterize gold nanoparticles (AuNPs), nanozymes (NZs), polymeric nanoparticles (PNPs) and polyzymes (PZs) (Section 3) are here exploited in order to get information about the dimensions and sizes of the pH-responsive polyzymes.
Transmission Electron Microscopy (TEM) and Dynamic Light Scattering (DLS) will be used to analyze the size of the polyzyme before and after the encapsulation of the catalyst to detect any possible aggregation of the polyzyme. Further size distribution studies for the polyzyme at a range of pH (4.5–7.4) using DLS will be performed in order to demonstrate their stability in acidic conditions.
The pH-responsive activity of the polyzyme will be validated via measurement of surface zeta potential at different pH values.
The loading capacity will be quantified using Inductively Coupled Plasma Mass Spectrometry (ICP-MS). Afterwards, catalytic efficiency will be measured through pro-resorufin activation.
First, the non-fluorescent pro-fluorophore molecule will be used as substrate and was activated to fluorescent molecule (resorufin) in the presence of [Fe(TPP)]Cl catalyst. Then, in order to demonstrate the ability of the polyzyme to allow the penetration of the hydrophobic metal catalyst inside the biofilm, that means that the polyzyme is able to create a path in the dense EPS matrix of the biofilm allowing the iron-porphyrin to penetrate inside it, Confocal Laser Scanning Microscopy (CLSM) will be used.
GFP-expressing *E. Coli* (CD-2) biofilms will be incubated with the pH-switchable polyzyme demonstrating that the embedded transition metal catalysts (TMCs) can activate pro-fluorophores *in situ* inside the biofilms.

Before studying the biofilm viability, the cytotoxity of the polyzyme towards mammalian cells should be measured by using Alamar Blue assay. After cytotoxity tests, the MBIC (Minimum Biofilm Inhibitory Concentration) and the MBEC (minimum Biofilm Eradication Concentration) can be perfomed in order to get the minimum concentration of the new functionalized polyzyme that could be toxic to the biofilm.
Once the MBEC is known, the pro-drug activation through the polyzyme inside the biofilm can be carried out by the Alamar Blue assay. The procedure could be like before (Section 5.2.3): *E. Coli* (CD-2) biofilms will be incubated with pH-responsive polyzyme and different concentrations of pro-drug, analysing the toxicity of the activated drug.
High biofilm viability in presence of pro-drug only and an extremely low viability in presence of both polyzyme and pro-drug are expected.

6.1.2 *Biofilm Study in an in vitro co-culture model*

To test the targeting ability of the pH-responsive polyzyme, this nanocatalyst can be employed in a biofilm-mammalian cell co-culture model (Figure 37).

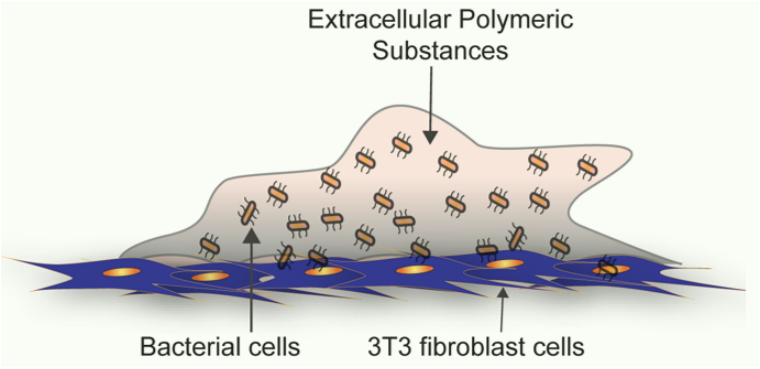

Figure 37: Schematic representation of biofilm-mammalian cell co-culture model.

In a multi-chamber culture disk, a total of 20,000 NIH-3T3 cells will be cultured for 24 h to reach a confluent monolayer [68]. NIH-3T3 cells are a continuous cell line of high contact-inhibition established from NIH Swiss mouse embryo cultures. The cells are useful for DNA transfection and transformation studies [69].
Afterwards, the bacteria (GFP (Green Fluorescent Protein)-expressing *E. Coli*) will be seeded overnight for biofilm formation.
Co-culture model will then be treated with polyzymes, followed by three washings using PBS to remove the non-adhesive polyzymes. Following this, the biofilm will be incubated with the pro-resorufin followed by other three washings using PBS again.
Finally, Confocal Laser Scanning Microscopy (CLSM) will be used to examine the spatial distribution of resorufin activation mediated by polyzymes. A strong colocalization of resorufin and GFP-expressing *E. Coli* biofilms and minimal fluorescence around mammalian cells are expected.

Following confocal studies, the therapeutic efficacy of the system has to be validated. *E. Coli* (CD-2) biofilm will be inoculated on NIH-3T3 cells to grow biofilms as mentionated above. After incubating with the polyzymes, different concentration of pro-Moxifloxacin will be added. Biofilms will be treated with pro-Moxifloxacin, only Moxifoxacin and a combination of pro-Moxifloxacin and polymer respectively as control groups. After 6 h of incubation, biofilm viability will be measured by Alamar Blue assay while cell viability will be analyzed with Lactate Dehydrogenase (LDH) assay. LDH is a common method for determining cytotoxycity based on measuring the activity

of cytoplasmic enzymes released by damaged cells [70].
The expectation is that the biofilm will be eradicated while no toxicity will be shown to mammalian cells.

6.2 MAXIMIZE THERAPEUTIC EFFICACY BY MULTI-DRUG ACTIVATION

To enhance therapeutic efficacy and expand the antimicrobial spectrum of the polyzyme, it can be interesting to focus on the combination therapy via multi-drug activation [71].
A strategy to enhance the efficacy of the polyzymes is to use them in combination with pro-antibiotics to eradicate biofilms.

For the initial therapy of severe infections, polyzyme mediated multi-drug activation will be able to create a broad-spectrum antimicrobial coverage and thus combats multi-species biofilms [72].
In addition, different activated drugs can function synergystically: the interaction between two or more drugs could probably make the total effect of the drugs greater than the sum of the individual effects of each drug.
The drug synergysm should show an increasing anti-biofilm efficacy and therefore a reducing dose-mediated toxicity.

6.2.1 *Selection and Fabrication of pro-drugs*

Initial studies will be focused on the synthesis of pro-drugs derived from antibiotics that have previously been used in combination therapies. The choice is based on the psycochemical properties of the drugs such as *lipophilicity*, as the ability of a molecule to interact with an oil phase, and *hydrophobicity*, as the ability to interact with the water [59]. Both of them are commonly measured by the $\log(P)$ value: the partition coefficient, abbreviated P, is defined as a particular ratio of the concentrations of a solute between two phases, and the logarithm of this ratio is thus $\log(P)$ [60]:

$$\log(P)_{oct/wat} = \log\left(\frac{[solute]^{un\text{-}ionized}_{octanol}}{[solute]^{un\text{-}ionized}_{water}}\right) \tag{3}$$

Synthesized pro-drugs should be hydrophobic enough to ensure high affinity to the catalyst in the hydrophobic pocket of the polyzyme but not too high hydrophobic, which will render the molecule insoluble.

Based on these considerations, Sulfamethoxazole ($\log(P) = 0.89$), a sulfonamide bacteriostatic antibiotic, combined with Ciprofloxacin

(log(P) = 0.28), a second generation fluoroquinolone antibiotic, will be used (Figure 38).

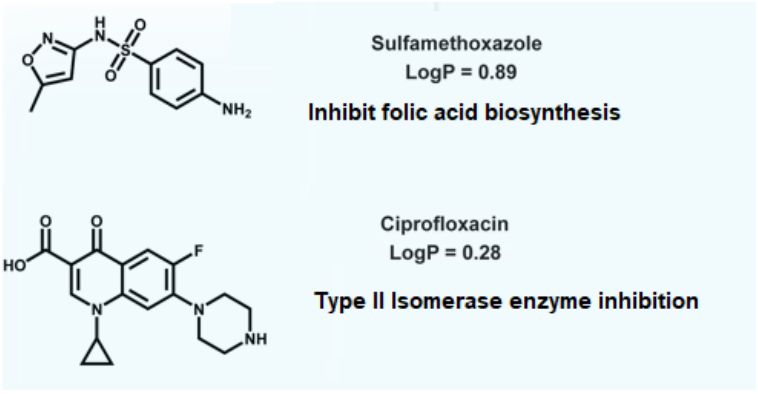

Figure 38: Selected antibiotics: Sulfamethoxazole (log(P) = 0.89) and Ciprofloxacin (log(P) = 0.28).

Sulfamethoxazole acts as a competitive inhibitors of the enzyme dihydropteroate synthase (DHPS), a precursor of the folic acid which is required for bacterial growth.
Ciprofloxain is a synthetic broad spectrum fluoroquinolone antibiotic able to bind and inhibit bacterial DNA gyrase, an enzyme essential for DNA replication [73].
These drugs will be converted into pro-drugs (Figure 39) through a functionalization of their amino groups to block the binding to the target enzyme.

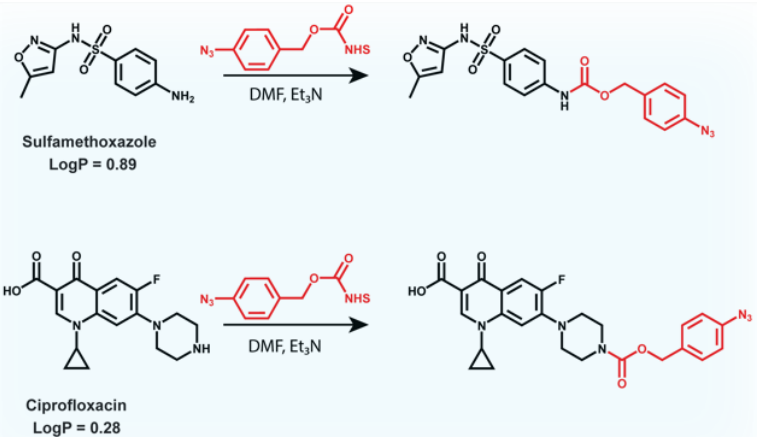

Figure 39: Synthesis of pro-drugs: pro-Sulfamethoxazole and pro-Ciprofloxacin [74].

Once the synthesis of pro-drugs will be completed, susceptibility tests will be performed on both drugs and pro-drugs to determine their minimum biofilm inhibitory concentration (MBIC) and

minimum biofilm eradication concentration (MBEC). Following this, the efficiency of the activation individually through HPLC (High-Performance Liquid Chromatography) will be monitored. HPLC is a modern technique able to identify, quantify and separate each component in a mixture. HPLC data should confirm the biochemical transformation of pro-drugs to their toxic counterparts.

6.2.2 *Testing of combination therapy*

The efficacy of multi-drug activation will be quantified on *E. Coli* (CD-2) biofilms. A widely accepted method to analyze the effect of combined therapeutic agents is to measure fractional biofilm eradication concentrantion (FBEC) index [75]. The FBEC index is used to identify whether a combination therapy is synergistic, additive, or antagonist. First, biofilms will be incubated with pH-responsive polyzyme in M9 media and subsequently washed multiple times using PBS.
Following this, the MBIC and the MBEC of pro-drugs subsequently activated through bioorthogonal catalysis will be evaluated. To evaluate FBEC, multi-drug activation will be tested by a checkboard titration method by running each well of a 96-well plate with different ratio of drugs [76]. According to this method it is possible to find not only the optimal concentration of each, but the optimal ratio of concentrations as well.

6.2.3 *Testing of efficacy of combination therapy in an in vitro co-culture model*

Evaluation of the therapeutic efficacy of multidrug activation will be performed in a similar method described above (Section 6.1.2) by exploiting polyzymes in a biofilm-mammalian cell co-culture model.
E. Coli (CD-2) bacteria will be inoculated on NIH-3T3 cells to grow biofilms. After incubating with pH-responsive polyzyme, combination of pro-drugs will be added.
Biofilms will be treated with pro-drugs, only drugs and a combination of pro-drugs and polymer respectively as control groups. After 6 h of incubation, biofilm viability will be determined by colony counting while cell viability will be analyzed with Lactate Dehydrogenase (LDH) assay.
The expectation is that the biofilm will be eradicated while no toxicity will be shown to mammalian cells.

7

CONCLUSIONS

The field of bioorthogonal chemistry is rapidly growing and has presented itself as an efficient tool for numerous applications including drug delivery and imaging.
Introducing bioortogonal catalysis to the polymeric scaffold and making polyzymes have paved ways to create efficient systems that can function in ways that are analogous to natural enzymes.
Transition metal catalysts (TMCs), despite of their promising role in catalysis, pose a major risk of toxicity due to the presence of heavy metals. The encapsulation of these TMCs into nanometric scaffold reduces the toxicity to some extent and also provides stability and solubility to the scaffold. The protection of TMCs in polymeric nanoparticles (PNPs) also circumvents the side effects of off-targeting that might arise due to passive diffusion of the catalysts.

Herein, a polymer-based nanocatalyst (polyzyme) for the treatment of bacterial biofilms is proposed. Through engineering the polymeric vehicle, it is possible to specifically deliver TMCs into biofilms providing a hydrophobic pocket for the protection of these catalysts. The fabricated polyzymes efficiently catalyze the formation of an active fluorophore under physiological conditions.
The polyzyme can be used as a smart system that efficiently generates antibiotics following the administration of pro-drugs.
In addition, the efficacy of this strategy can be enhanced by functionalizing the polyzyme surface for the activation of pro-antibiotics at the target site. Furthermore, the polzyme activity can be exploited for multi-drug activation.
This would be really helpful to minimize antibiotic-induced resistance of the biofilm against treatments. This polyzyme platform provides a modular toolkit to perform bioorthogonal reactions with precise control while maintaining high efficiency. The polyzyme here is a potentially powerful tool to combat bacterial biofilm-associated infections.
The research in the field of polyzymes has been constantly evolving. Prospective developments in this field of research would establish the use of these novel bioorthogonal catalysts in a range of wide applications by surmounting the potential challenges.

BIBLIOGRAPHY

[1] A. Gupta et al. "Engineered Polymer Nanoparticles with Unprecedented Antimicrobial Efficacy and Therapeutic Indices against Multidrug-Resistant Bacteria and Biofilms." In: *Journal of the American Chemical Society* 140.38 (2018), pp. 12137–12143.

[2] W. R. Algar et al. "The Controlled Display of Biomolecules on Nanoparticles: A Challenge Suited to Bioorthogonal Chemistry." In: *Bioconjugate Chemistry* 22.5 (2011), pp. 825–858.

[3] V. A. Prof. Cauda. *Theranostic Nanomaterials from "Physical properties at nanoscale, nanomanipulations and nanoprocessi"*. 2016-17.

[4] G. Y. Tonga et al. "Supramolecular regulation of bioorthogonal catalysis in cells using nanoparticle-embedded transition metal catalysts." In: *Nature Chemistry* 7 (2015), pp. 597–603.

[5] E. M. Sletten and C. R. Bertozzi. "Bioorthogonal chemistry: fishing for selectivity in a sea of functionality." In: *Angewandte Chemie International Edition* 48.38 (2009), pp. 6974–98.

[6] R. M. Versteegen et al. "Click to Release: Instantaneous Doxorubicin Elimination upon Tetrazine Ligation." In: *Angewandte Chemie International Edition* 52.52 (2013), pp. 14112–14116.

[7] T. Völker and E. Meggers. "Transition-metal-mediated uncaging in living human cells—an emerging alternative to photolabile protecting groups." In: *Current Opinion in Chemical Biology* 25 (2015), pp. 48–54.

[8] C. Streu and E. Prof. Meggers. "Ruthenium-Induced Allylcarbamate Cleavage in Living Cells." In: *Angewandte Chemie International Edition* 45.34 (2006), pp. 5645–5648.

[9] X. Zhang et al. "Bioorthogonal Nanozymes: Progress towards Therapeutic Applications." In: *Cell Press Reviews* 1.1 (2019), pp. 90–98.

[10] J. A. Prescher and C. R. Bertozzi. "Chemistry in living systems." In: *Nature Chemical Biology* 1.1 (2005), pp. 13–21.

[11] E. M. Sletten and C. R. Bertozzi. "From Mechanism to Mouse: A Tale of Two Bioorthogonal Reactions." In: *Accounts of Chemical Research* 44.9 (2011), pp. 666–676.

[12] P. S. Sasmal, C. Streub, and E. Meggers. "Metal complex catalysis in living biological systems." In: *Chemical Communications* 16.49 (2013), pp. 1581–1587.

[13] A. Unciti-Broceta et al. "Synthesis of polystyrene microspheres and functionalization with Pd(0) nanoparticles to perform bioorthogonal organometallic chemistry in living cells." In: *Nature Protocols* 7.6 (2012), pp. 1207–18.

[14] J. Li et al. "Palladium-triggered deprotection chemistry for protein activation in living cells." In: *Nature Chemistry* 6.4 (2014), pp. 352–361.

[15] J. T. Weiss et al. "Extracellular palladium-catalysed dealkylation of 5-fluoro-1-propargyl-uracil as a bioorthogonally activated prodrug approach." In: *Nature Communications* 5.1 (2014).

[16] M. I. Sánchez et al. "Metal-catalyzed uncaging of DNA-binding agents in living cells." In: *Chemical Science* 5 (2014), pp. 1901–1907.

[17] S. Alonso-deCastro et al. "Bioorthogonal Catalytic Activation of Platinum and Ruthenium Anticancer Complexes by FAD and Flavoproteins." In: *Angewandte Chemie International Edition* 57 (2018), pp. 3143–3147.

[18] P. K. Dr. Sasmal et al. "Catalytic Azide Reduction in Biological Environments." In: *ChemBioChem* 13.8 (2012), pp. 1116–20.

[19] A. Gupta et al. "Charge-Switchable Nanozymes for Bioorthogonal Imaging of Biofilm-Associated Infections." In: *ACS Nano* 12.1 (2018), pp. 89–94.

[20] Z. Huma et al. "Cationic Silver Nanoclusters as Potent Antimicrobials against Multidrug-Resistant Bacteria." In: *ACS Omega* 3.12 (2018), pp. 16721–16727.

[21] R. Das et al. "Control of Intra- versus Extracellular Bioorthogonal Catalysis Using Surface-Engineered Nanozymes." In: *ACS Nano* 13.1 (2019), pp. 229–235.

[22] A. Gupta et al. "Charge-Switchable Nanozymes for Bioorthogonal Imaging of Biofilm-Associated Infections." In: *ACS Nano* 12.1 (2018), pp. 89–94.

[23] H.-C. Flemming et al. "Biofilms: an emergent form of bacterial life." In: *Nature Reviews Microbiology* 14.9 (2016), pp. 563–75.

[24] MicrobeWiki. *Biofilms and Human Implants*. https://microbewiki.kenyon.edu/index.php/Biofilms_and_Human_Implants.

[25] R. Mohankandhasamy and J. Lee. "Recent Nanotechnology Approaches for Prevention and Treatment of Biofilm-Associated Infections on Medical Devices." In: *BioMed Research International* 46.2 (2016), pp. 1–17.

[26] N. S. Chandel and G. R. S. Budinger. "The Good and the Bad of Antibiotics." In: *Science Translational Medicine* 5.192 (2013).

[27] Y. Liu et al. "Catalytically Active Single-Chain Polymeric Nanoparticles: Exploring Their Functions in Complex Biological Media." In: *Journal of the American Chemical Society* 140.9 (2018), pp. 3423–3433.

[28] P. S. Stewart and J. Costerton. "Antibiotic resistance of bacteria in biofilms." In: *The Lancet* 358.9276 (2001), pp. 135–138.

[29] J. N. Anderl, M. Franklin, and P. Stewart. "Role of antibiotic penetration limitation in Klebsiella pneumoniae biofilm resistance to ampicillin and ciprofloxacin." In: *Antimicrobial Agents and Chemotherapy* 44.7 (2000), pp. 1818–24.

[30] X. Zhang et al. "Palladium(II)N-Heterocyclic Carbene Metallacrown Ether Complexes: Synthesis, Structure, and Catalytic Activity in the SuzukiMiyaura Reaction." In: *Organometallics* 28.10 (2009), pp. 3093–3099.

[31] L.-A. Schaper et al. "Synthesis and Application of Water-Soluble NHC Transition-Metal Complexes." In: *Angewandte Chemie International Edition* 52.1 (2013), pp. 207–289.

[32] M. Tomás-Gamasa et al. "Transition metal catalysis in the mitochondria of living cells." In: *Nature Communications* 7.12538 (2016).

[33] H. Wei and E. Wang. "Nanomaterials with enzyme-like characteristics (nanozymes): next-generation artificial enzymes." In: *Chemical Society Reviews* 42.14 (2013), pp. 6060–6093.

[34] J. Wu et al. "Nanomaterials with enzyme-like characteristics (nanozymes): next-generation artificial enzymes (II)." In: *Chemical Society Reviews* 48.4 (2019), pp. 1004–1076.

[35] Y. Jeong et al. "Solubilization of Hydrophobic Catalysts Using Nanoparticle Hosts." In: *Small* 14.7 (2018).

[36] A. Hu, S. Liu, and W. Lin. "Immobilization of chiral catalysts on magnetite nanoparticles for highly enantioselective asymmetric hydrogenation of aromatic ketones." In: *RSC Advances* 2.6 (2012), pp. 2576–2580.

[37] J. M. Thomas et al. "Nanoporous oxidic solids: the confluence of heterogeneous and homogeneous catalysis." In: *Physical Chemistry Chemical Physics* 11.16 (2009), pp. 2799–2825.

[38] L. Xiaoning et al. "Control of nanoparticle penetration into biofilms through surface design." In: *Chemical Communications* 2.51 (2015), pp. 282–285.

[39] R. H. Grubbs and W. Tumas. "Polymer synthesis and organotransition metal chemistry." In: *Science* 243.4893 (1989), pp. 907–915.

[40] J.-L. P. Hérisson and Y. Chauvin. "Catalyse de transformation des oléfines par les complexes du tungstène. II. Télomérisation des oléfines cycliques en présence d'oléfines acycliques." In: *Die Makromolekulare Chemie* 141.1 (1971), pp. 161–176.

[41] P. Ghosh et al. "Gold nanoparticles in delivery applications." In: *Advanced Drug Delivery Reviews* 60.11 (2008), pp. 1307–1315.

[42] A. C. Templeton, W. P. Wuelfing, and R. Murray. "Monolayer-Protected Cluster Molecules." In: *Accounts of Chemical Research* 33.1 (2000), pp. 27–36.

[43] M. Brust et al. "Synthesis of Thiol-derivatised Gold Nanoparticles in a Two-phase Liquid-Liquid System." In: *Journal of the Chemical Society, Chemical Communications* 7 (1994), pp. 801–802.

[44] G. Y. Tonga. "Nanoparticle as supramolecular platform for delivery and bioorthogonal catalysis." PhD thesis. 2017.

[45] Y. Liu et al. "Catalytically Active Single-Chain Polymeric Nanoparticles: Exploring Their Functions in Complex Biological Media." In: *Journal of the American Chemical Society* 140.9 (2018), pp. 3423–3433.

[46] A. E. Madkour et al. "End-Functionalized ROMP Polymers for Biomedical Applications." In: *Macromolecules* 43.10 (2010), pp. 4557–4561.

[47] F. Prof. Giorgis. *Transmission Electron Microscopy notes from "Micro Electro Mechanical Sistems"*. 2016-17.

[48] Wikipedia. *Transmission electron microscopy*. https://en.wikipedia.org/wiki/Transmission_electron_microscopy.

[49] Britannica. *Transmission electron microscope*. https://www.britannica.com/technology/transmission-electron-microscope.

[50] M. Panalytical. *Dynamic Light Scattering: An Introduction in 30 Minutes*. https://warwick.ac.uk/fac/cross_fac/sciencecity/programmes/internal/themes/am2/booking/particlesize/intro_to_dls.pdf.

[51] C. Eberhard. "Development of a Model System to Study Cell Adhesion and Cell Mechanics." PhD thesis. 2012.

[52] T. Völker et al. "Progress towards Bioorthogonal Catalysis with Organometallic Compounds." In: *Angewandte Chemie International Edition* 53 (2014), pp. 1–6.

[53] O. Shimomura, F. Johnson, and Y. Saiga. "Extraction, purification and properties of aequorin, a bioluminescent protein from the luminous hydromedusan, Aequorea." In: *Journal of Cellular and Comparative Physiology* 59.3 (1962), pp. 223–39.

[54] R. Y. Tsien. "The green fluorescent protein." In: *Annual Review of Biochemistry* 67 (1998), pp. 509–44.

[55] G. Zhang, V. Gurtu, and S. Kain. "An Enhanced Green Fluorescent Protein Allows Sensitive Detection of Gene Transfer in Mammalian Cells." In: *Biochemical and Biophysical Research Communications* 227.3 (1996), pp. 707–711.

[56] R. A. G. Cinelli et al. "The Enhanced Green Fluorescent Protein as a Tool for the Analysis of Protein Dynamics and Localization: Local Fluorescence Study at the Single-molecule Level." In: *Photochemistry and Photobiology* 71.6 (2000), pp. 771–776.

[57] Wikipedia. *Pathogenic Escherichia coli*. https://en.wikipedia.org/wiki/Pathogenic_Escherichia_coli#Role_in_disease.

[58] C. M. Oliphant and G. M. Green. "Quinolones: a comprehensive review." In: *American Family Physician* 65.3 (2002), pp. 455–64.

[59] L. Di and E. Kerns. *Drug-like properties*. Ed. by A. Press. 2nd ed. 2016.

[60] Wikipedia. *Partition coefficient*. https://en.wikipedia.org/wiki/Partition_coefficient.

[61] QLaboratories. *Minimum Inhibitory (MIC) and Minimum Bactericidal Concentration (MBC) Evaluations as RD Tools*. https://www.qlaboratories.com/minimum-inhibitory-mic-and-minimum-bactericidal-concentration-mbc-evaluations-as-rd-tools/.

[62] emery pharma. *Biofilm Eradication Testing*. https://emerypharma.com/biology/biofilm-eradication/.

[63] wikipedia. *Minimum bactericidal concentration*. https://en.wikipedia.org/wiki/Minimum_bactericidal_concentration.

[64] T. Fisher. *alamarBlue Assay*. https://www.thermofisher.com/order/catalog/product/DAL1025#/DAL1025.

[65] H. Koo et al. "Targeting microbial biofilms: current and prospective therapeutic strategies." In: *Nature Reviews Microbiology* 15.12 (2017), pp. 740–755.

[66] D. S. W. Benoit and H. Koo. "Targeted, triggered drug delivery to tumor and biofilm microenvironments." In: *Nanomedicine* 11.8 (2016), pp. 873–9.

[67] T. Mizuhara et al. "Acylsulfonamide-Functionalized Zwitterionic Gold Nanoparticles for Enhanced Cellular Uptake at Tumor pH." In: *Angewandte Chemie International Edition in English* 54.22 (2015), pp. 6567–6570.

[68] C. Weidenmaier et al. "Role of teichoic acids in Staphylococcus aureus nasal colonization, a major risk factor in nosocomial infections." In: *Nature Medicine* 10.3 (2004), pp. 243–5.

[69] N. C. for Biotechnology Information. *NIH 3T3 Cells*. https://www.ncbi.nlm.nih.gov/mesh/68041681.

[70] P. Kumar, A. Nagarajan, and P. Uchil. "Analysis of Cell Viability by the Lactate Dehydrogenase Assay." In: *Cold Spring Harbor Protocols* (2018).

[71] M. A. Fischbach. "Combination therapies for combating antimicrobial resistance." In: *Current Opinion in Microbiology* 14.5 (2011), pp. 519–523.

[72] H. C. Neu. "Synergy and antagonism of combinations with quinolones." In: *European Journal of Clinical Microbiology Infectious Diseases* 10.4 (1991), pp. 255–61.

[73] J. A. Katie, R. Kerns, and N. Osheroff. "Mechanism of Quinolone Action and Resistance." In: *Biochemistry* 53.10 (2014), pp. 1565–1574.

[74] D. Wojciechowski and S. Chandran. "Effect of Ciprofloxacin Combined with Sulfamethoxazole-Trimethoprim Prophylaxis on the Incidence of Urinary Tract Infections After Kidney Transplantation." In: *Transplantation Journal* 96.4 (2013), pp. 400–405.

[75] D. S. Burgess, R. Hall, and T. Hardin. "In vitro evaluation of the activity of two doses of Levofloxacin alone and in combination with other agents against Pseudomonas aeruginosa." In: *Diagnostic Microbiology and Infectious Disease* 46.2 (2003), pp. 131–7.

[76] S. Bajaksouzian et al. "Activities of levofloxacin, ofloxacin, and ciprofloxacin, alone and in combination with amikacin, against acinetobacters as determined by checkerboard and time-kill studies." In: *Antimicrobial Agents and Chemotherapy* 41.5 (1997), pp. 1073–6.